Intermediates and Transition States in Thiamin Diphosphate-Dependent Decarboxylases. A Kinetic and NMR Study on Wild-Type Indolepyruvate Decarboxylase and Variants Using Indolepyruvate, Benzoylformate, and Pyruvate as Substrates†

Anja Schütz, Ralph Golbik, Stephan König, Gerhard Hübner, and Kai Tittmann*

Institut für Biochemie, Fachbereich Biochemie/Biotechnologie, Martin-Luther-Universität Halle-Wittenberg, Kurt-Mothes-Strasse 3, 06099 Halle/Saale, Germany

Received December 20, 2004; Revised Manuscript Received February 1, 2005

ABSTRACT: The thiamin diphosphate (ThDP)-dependent enzyme indolepyruvate decarboxylase (IPDC) is involved in the biosynthetic pathway of the phytohormone 3-indoleacetic acid and catalyzes the nonoxidative decarboxylation of 3-indolepyruvate to 3-indoleacetaldehyde and carbon dioxide. The steady-state distribution of covalent ThDP intermediates of IPDC reacting with 3-indolepyruvate and the alternative substrates benzoylformate and pyruvate has been analyzed by ^{1}H NMR spectroscopy. For the first time, we are able to isolate and directly assign covalent intermediates of ThDP with aromatic substrates. The intermediate analysis of IPDC variants is used to infer the involvement of active site side chains and functional groups of the cofactor in distinct catalytic steps during turnover of the different substrates. As a result, three residues (glutamate 468, aspartate 29, and histidine 115) positioned perpendicular to the thiazolium moiety of ThDP are involved in binding of all substrates and decarboxylation of the respective tetrahedral ThDP−substrate adducts. Most likely, interactions of these side chains with the substrate-derived carboxylate account for an optimal orientation of the substrate and/or intermediate in the course of carbon−carbon ligation and decarboxylation supporting the suggested least-motion, maximum overlap mechanism. The active site residue glutamine 383, which is located at the opposite site of the thiazolium nucleus as the "carboxylate pocket" (formed by the Glu-Asp-His triad), is central to the substrate specificity of IPDC, probably through orbital alignment. The Glu51−cofactor proton shuttle is, conjointly with the Glu-Asp-His triad, involved in multiple proton transfer steps, including ylide generation, substrate binding, and product release. Studies with para-substituted benzoylformate substrates demonstrate that the electronic properties of the substrate affect the stabilization or destabilization of the carbanion intermediate or carbanion-like transition state and in that way alter the rate dependence on decarboxylation. In conclusion, general mechanistic principles of catalysis of ThDP-dependent enzymes are discussed.

Indolepyruvate decarboxylase (IPDC,[1] EC 4.1.1.74) from *Enterobacter cloacae* belongs to the family of cofactor-dependent enzymes that utilize thiamin diphosphate (ThDP) as the biologically active derivative of vitamin B_1. In some plant-associated microorganisms such as *E. cloacae*, IPDC is a key enzyme for the biosynthesis of the plant growth regulator 3-indoleacetic acid and catalyzes the conversion of 3-indolepyruvate (Ipyr), which primarily originates from L-tryptophan, to carbon dioxide and 3-indoleacetaldehyde (*1*−*3*). Recent kinetic studies showed that pyruvate (Pyr), benzoylformate (BF), and several para-substituted BFs are also substrates of IPDC (*4*). Although IPDC displays the highest catalytic efficiency (k_{cat}/K_M) for the physiological substrate Ipyr, the catalytic constant (k_{cat}) of BF turnover (11.6 s^{-1}) is approximately 10 times higher than those of Ipyr (0.98 s^{-1}) and Pyr (0.88 s^{-1}).

The X-ray crystallographic structure of IPDC evidenced a high structural similarity of IPDC and pyruvate decarboxylase from *Zymomonas mobilis* (*Zm*PDC, EC 4.1.1.1) (*5*, *6*). As illustrated in a superimposition of the active sites of both enzymes (Figure 1A), the enzyme-bound cofactor and an array of conserved amino acid side chains (Glu468···Asp29···His115···Glu52 in IPDC and Glu473···Asp27···His113···Glu50 in *Zm*PDC) occupy nearly identical positions in the active sites of both enzymes. The different substrate

† This work was supported by the Fonds der Chemischen Industrie.

* To whom correspondence should be addressed. E-mail: kai@bc.biochemtech.uni-halle.de. Phone: +49-345-5524887. Fax: +49-345-5527014.

[1] Abbreviations: IPDC, indolepyruvate decarboxylase (EC 4.1.1.74); *Sc*PDC, pyuvate decarboxylase (EC 4.1.1.1) from *Saccharomyces cerevisiae*; *Zm*PDC, pyruvate decarboxylase (EC 4.1.1.1) from *Z. mobilis*; BFDC, benzoylformate decarboxylase (EC 4.1.1.7); Pyr, pyruvate; Ipyr, 3-indolepyruvate; BF, benzoylformate; ThDP, thiamin diphosphate; $ThDP^-$, carbanion form of ThDP; LThDP, 2-lactyl-ThDP; HEThDP, 2-(1-hydroxyethyl)-ThDP; $HETHDP^-$, carbanion/enamine form of HEThDP; MThDP, 2-mandelyl-ThDP; HBzThDP, 2-(1-hydroxybenzyl)-ThDP; $HBzThDP^-$, carbanion/enamine form of HBzThDP; IndLThDP, 2-(3-indolyl-(3)-lactyl)-ThDP; IndHEThDP, 2-(1-hydroxy-2-indolyl-(3)-ethyl)-ThDP; $IndHEThDP^-$, carbanion/enamine form of IndHEThDP; substrate−ThDP, tetrahedral substrate−ThDP adduct (LThDP, MThDP, IndLThDP); product−ThDP, tetrahedral product−ThDP adduct (HEThDP, HBzThDP, IndHEThDP); AHAS, acetohydroxyacid synthase; POX, pyruvate oxidase; TK, transketolase; PFOR, pyruvate:ferredoxin oxidoreductase.

10.1021/bi0473354 CCC: $30.25
Published on Web 04/02/2005

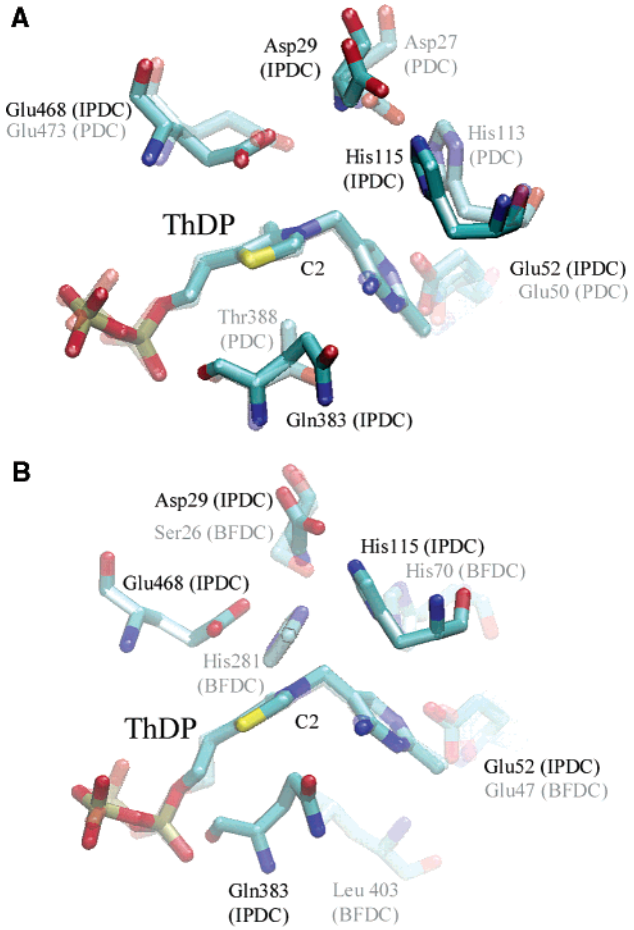

FIGURE 1: Superimposition of the active sites of IPDC (opaque) with PDC from *Z. mobilis* (transparent in panel A) and BFDC from *Pseudomonas putida* (transparent in panel B) showing the cofactor ThDP and selected amino acid residues (*5*−*7*). Spatial coordinates of ThDP were superimposed with a least-squares algorithm using VMD (*59*). Please note that no electron density for the C2 atom of ThDP has been observed in the X-ray structure of *Zm*PDC (*6*). The spatial coordinates of C2 were calculated from the positions of the remaining atoms of the thiazolium ring.

specificity has been associated with the nonconserved side chain glutamine 383 in IPDC and its homologue threonine 388 in *Zm*PDC.

A structural comparison of IPDC and benzoylformate decarboxylase (BFDC, EC 4.1.1.7) from *Pseudomonas putida* reveals some common characteristics as well as remarkable variations in the active site architecture (Figure 1B) (*5*, *7*). In both enzymes, the cofactor ThDP adopts the typical *V* conformation, and N1′ of the aminopyrimidine ring interacts with the side chain of a highly conserved glutamate (Glu52 in IPDC and Glu47 in BFDC). Despite some deviations in the spatial orientation, histidine 115 (IPDC) and histidine 70 (BFDC) may be regarded as conserved. The structural homologue of aspartate 29 (IPDC) is serine 26 (BFDC), a residue that apparently cannot provide for common acid/base chemistry. Aside from this, glutamate 468 (IPDC) and histidine 281 (BFDC) seem to have no direct equivalent.

The catalytic cycle of IPDC catalysis can be subdivided into several microscopic steps (Figure 2). Initially, C2 of the thiazolium ring of ThDP is deprotonated, forming the reactive ylide form of the cofactor ($ThDP^-$) (step 0). Subsequently, the substrate is lured into the active site (step 1), and the ylide attacks the substrate carbonyl forming the tetrahedral substrate−ThDP adduct (step 2). Depending on the substrate, this species can be termed 2-lactyl-ThDP (LThDP, substrate Pyr), 2-mandelyl-ThDP (MThDP, substrate BF), or 2-(3-indolyl-(3)-lactyl)-ThDP (IndLThDP, substrate Ipyr). This intermediate is decarboxylated (step 3) to the carbanion/enamine form of 2-(1-hydroxyethyl)-ThDP (HEThDP, substrate Pyr), 2-(1-hydroxybenzyl)-ThDP (HBzThDP, substrate BF), or 2-(1-hydroxy-2-indolyl-(3)-ethyl)-ThDP (IndHEThDP, substrate Ipyr). Liberation of the respective aldehyde requires the protonation of the carbanion/enamine (step 4a), deprotonation of the α-hydroxyl group, and cleavage of the carbon−carbon bond between C2 of ThDP and C_α of the intermediate (step 4b). For the sake of clarity, step 4 is shown to occur in a stepwise manner, although a concerted mechanism may be alternatively discussed.

Different methodological approaches have been successfully applied for a kinetic and mechanistic analysis of single steps in ThDP catalysis. For BFDC, transient stopped flow kinetics using the chromophoric substrate analogue *p*-nitrobenzoylformate together with the structure of the enzyme-bound inhibitor (*R*)-mandelate suggested His70 and Ser26 to be involved in substrate binding and decarboxylation, and His281 to be mandatory for the protonation of the carbanion/enamine (*8*, *9*). We recently introduced a combined acid quench/^{1}H NMR-based method that allows the quantitative analyses of covalent ThDP intermediates under steady-state conditions (*10*). Previous NMR studies on wild-type *Zm*PDC and active site variants confirmed the least motion, maximum overlap mechanism of decarboxylation as proposed by Kluger and others and indicated the involvement of two independent proton relays in the course of proton transfer steps (*10*−*15*).

In the studies presented here, we demonstrate that the ^{1}H NMR-based intermediate analysis can also be successfully applied for ThDP-dependent enzymes that act on aromatic substrates. In a case study on IPDC, key intermediates during turnover of aromatic substrates 3-indolepyruvate and benzoylformate and the aliphatic substrate pyruvate are directly detected and quantitatively analyzed. In addition to the wild-type enzyme, a set of active site variants has been characterized by means of classic kinetics and the NMR intermediate method. As a result, a functional assignment of side chains in single steps of catalysis is proposed and is discussed in the context to the recently presented mechanism of BFDC and PDC and relevant model studies.

MATERIALS AND METHODS

Reagents. Horse liver alcohol dehydrogenase was from Roche Molecular Biochemical Inc. Yeast alcohol dehydrogenase and NADH were purchased from Sigma-Aldrich Chemie GmbH. All other chemicals were obtained from VWR International GmbH, Sigma-Aldrich Chemie GmbH, Carl Roth GmbH, and AppliChem GmbH. Quartz double-distilled water was used throughout the experiments.

Site-Directed Mutagenesis. The active site mutants Asp29Glu, Glu52Asp, His115Lys, Gln383Thr, and Glu468Asp were generated using the QuikChange site-directed mutagenesis kit (Stratagene GmbH, Heidelberg, Germany). The PCR was carried out with 20 ng of wild-type plasmid DNA as a

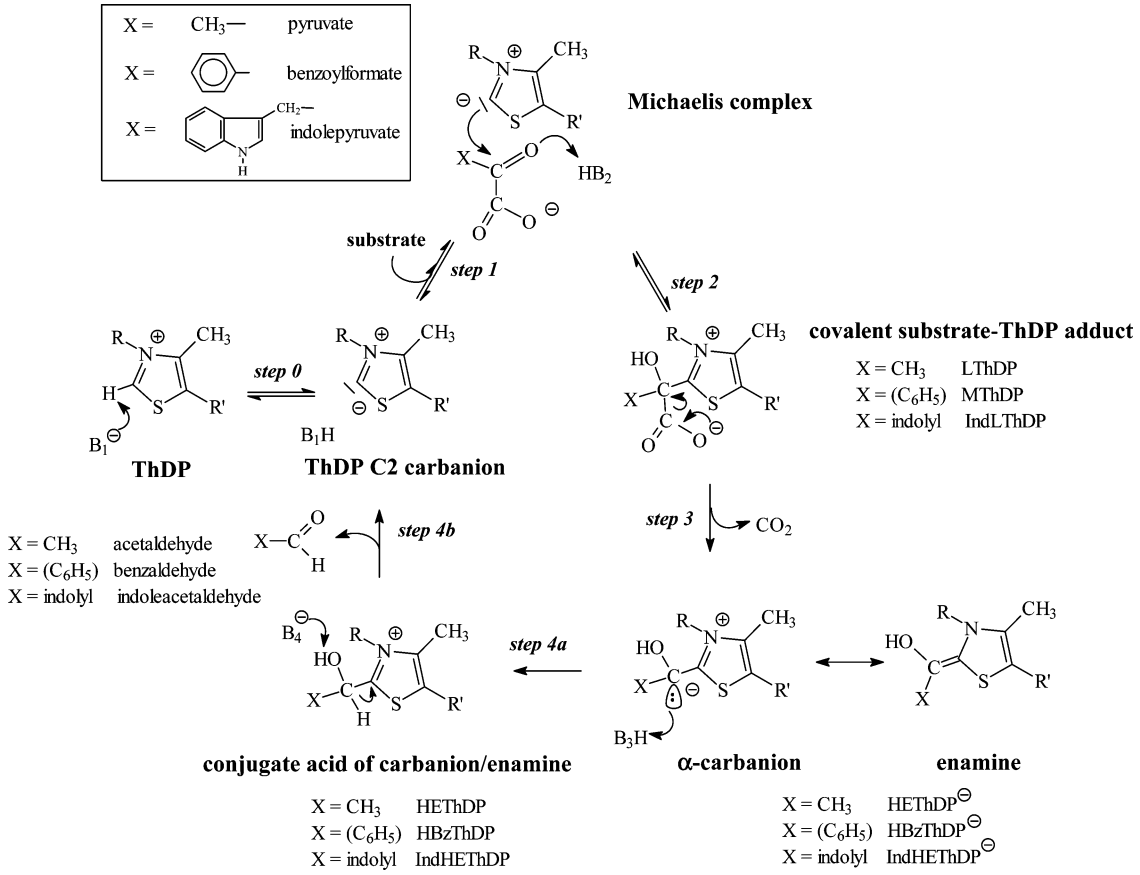

FIGURE 2: Catalytic cycle of IPDC with key intermediates invoked in nonoxidative decarboxylation of the substrates 3-indolepyruvate, benzoylformate, and pyruvate.

template and specific designed primers. For a fast initial screening of putative mutant clones, additional silent mutations were introduced creating new restriction sites. The forward primers used for the mutagenesis reaction are shown below with the mutated codons underlined, the codon of the exchanged amino acid in boldface type, and the new restriction site in parentheses: Asp29Glu, 5′-CAT CTG TTT GGC GTG CCC GGG **GAG** TAT AAC CTG CAG-3′ (*Sma*I); Glu52Asp, 5′-GTG GGC TGT GCC AAT **GAC** CTG AAT GCA TCC TAT GCC-3′ (*Bsm*I); His115Lys, 5′-AGG GGA GAG CTC CTG **AAG** CAT ACG TTG GGG GAT GGG GAG-3′ (*Sac*I); Gln383Thr, 5′-GAC ATT ATC CTT GCC GAC **ACG** GGT ACC TCG GCC TTC GGC-3′ (*Kpn*I); and Glu468Asp, 5′-GGT TAC ACG GTC **GAC** AGA GCT ATC CAC GGG GCG-3′ (*Sal*I).

The template DNA was removed by treatment with *Dpn*I, and the remaining PCR product was transformed into *Escherichia coli* strain JM 109 (*16*). Single colonies were picked and cultivated in liquid medium. The plasmid DNA of the clones was isolated using the QIAprep Spin Miniprep Kit (QIAGEN GmbH, Hilden, Germany) and screened for the desired mutation by restriction analysis with the respective restriction endonuclease (see above). The correctness of the mutation was confirmed by sequencing of the *Ec*IPDC coding nucleotide sequence using the ABI PRISM310 genetic analyzer (Applied Biosystems, Applera Deutschland GmbH, Darmstadt, Germany).

Cell Cultivation, Expression, and Protein Purification. Cell cultivation, gene expression, and protein purification of wild-type IPDC and variants have been carried out as described in ref *4*.

Determination of Protein Concentrations. The concentration of IPDC was determined spectrophotometrically at 280 nm using a calculated molecular absorption coefficient of 259 520 M^{-1} cm^{-1} (*4*). ThDP-containing protein samples were quantified by the method of Bradford (*17*).

Determination of the Catalytic Constants. The catalytic activity of IPDC was measured in a coupled optical test employing NADH and either horse liver alcohol dehydrogenase (substrates Ipyr and BF) or yeast alcohol dehydrogenase (substrate Pyr) as described in ref *4*.

The catalytic constants were calculated by fitting the experimental data according to the Michaelis−Menten equation. In the case of substrate excess inhibition, data were fitted according to eq 1:

$$v([S]) = \frac{V_{max}[S]}{[S]\left(1 + \frac{[S]}{K_i} + K_M\right)} \quad (1)$$

One unit is defined as the amount of enzyme converting 1 μmol of substrate per minute.

Synthesis of Para-Substituted Benzoylformates. Syntheses were carried out according to ref *18* by oxidation of the corresponding acetophenones by SeO_2.

Chemical and Enzymatic Synthesis of Covalent ThDP Adducts. The covalent ThDP adducts LThDP and HEThDP, being transient intermediates in the course of pyruvate conversion by IPDC, were chemically synthesized according to the protocols in refs *11* and *19*. HBzThDP, a key intermediate during enzymic decarboxylation of BF, has been

synthesized according to the methods of refs *20* and *21*. Purity and chemical stability under acidic conditions were analyzed by ^{1}H NMR spectroscopy.

In analogy to the protocol of HBzThDP synthesis, we attempted to prepare IndHEThDP. However, the chemical ligation of ThDP and 3-indoleacetaldehyde tends to proceed with extremely poor yields. Therefore, we synthesized this adduct enzymatically using the Asp29Glu IPDC variant. In the presence of Ipyr and excess ThDP-Mg^{2+}, this variant produces considerable amounts of IndHEThDP. A total of 1 mL of reaction mix containing 5 mg/mL IPDC Asp29Glu variant, 15 mM ThDP, 15 mM Mg^{2+}, and 5 mM Ipyr was incubated for 2 h at 25 °C in 200 mM MES-NaOH (pH 6.5). Thereafter, 50 μL of concentrated HCl (37%) was added, leading to instantaneous denaturation of the protein, which was removed by centrifugation at 15000*g* for 15 min at 4 °C. The supernatant was then adjusted to pH 5.5 using diluted NaOH and applied to a QAE-Sephadex A25 column previously established in the acetate form by 0.5 M sodium acetate (pH 6.7). Under the conditions that were used, ThDP and ThDP adducts bind to the ion exchange matrix. The substrates, products, and buffer compounds were removed by repeated washing with water. Elution of IndHEThDP and ThDP was accomplished by applying an isocratic gradient of 100 mL from 0 to 50 mM acetic acid. Fractions were collected in 2 mL quantities and subsequently analyzed by ^{1}H NMR spectroscopy. A description of the spectroscopic and chemical properties of IndHEThDP is given in the Results.

Steady-State Intermediate Analysis by ^{1}H NMR and H−D Exchange Kinetics at C2 of ThDP. Apo-IPDC (15 mg/mL, 250 μM active sites) was reconstituted with an equimolar amount of ThDP and 5 mM Mg^{2+} in 200 mM MES-NaOH (pH 6.5) at 30 °C for 10 min. Under these conditions, all active sites are occupied by ThDP, because no increase in activity can be observed after addition of excess ThDP (1 mM), neither for the wild-type enzyme nor for the variants. Therefore, the fraction of unbound ThDP is negligible within experimental error (<5%). Depending on the substrate and the substrate-specific catalytic constants (K_M and k_{cat}) of the variant that was being investigated, the enzyme was mixed with a saturating concentration of the respective substrate for defined reaction times (assured steady-state conditions) in 100 mM MES-NaOH (pH 6.5) at 30 °C, either by using a rapid quench flow device (RQF-3, Kintek Althouse) for reaction times up to 2000 ms or by manual mixing for longer reaction times. The reaction was quenched by the addition of 12.5% (w/v) TCA and 1 M DCl (in D_2O). The denatured protein was discarded after centrifugation, and the supernatant containing the intermediates, substrates, and products was analyzed by ^{1}H NMR spectroscopy.

For the assignment and quantitative analysis of ThDP and covalent ThDP adducts (see the Results), the C6′-H ^{1}H NMR signals of ThDP (8.01 ppm), LThDP (7.27 ppm), HEThDP (7.33 ppm), MThDP (6.72 ppm), HBzThDP (6.61 ppm), IndLThDP (6.8 ppm), and IndHEThDP (6.37 ppm) were used. Since the aromatic proton signals of the substrates Ipyr and BF interfere with that of C6′-H of ThDP, the C2-H resonance of ThDP was deployed for analysis in that case. NMR aquisition and data processing were carried out as described in ref *10*.

For the calculation of the unimolecular net rate constants of single steps of catalysis, the following minimal catalytic scheme is assumed comprising (i) the reversible, noncovalent binding of the substrate (K_1), (ii) the formation of the covalent substrate−ThDP adduct (k_2'), (iii) the decarboxylation of the intermediate to the enamine/carbanion (k_3'), and (iv) product release (k_4'). Noteworthy is the fact that the acid quench/NMR analysis does not allow a discrimination of the carbanion/enamine and its conjugate acid because of the instantaneous protonation of the carbanion/enamine after its release from the active site. Therefore and irrespective of a concerted or stepwise product release, k_4' represents the protonation of the carbanion/enamine, the deprotonation of the hydroxyl group, and C2−C_α bond cleavage.

$$\text{E−ThDP} + \text{substrate (Ipyr, BF, Pyr)} \xrightarrow{K_1} \text{E−ThDP*substrate (Michaelis complex)} \quad (2)$$

$$\text{E−ThDP*substrate} \xrightarrow{k_2'} \text{E−ThDP−substrate (IndLThDP/MThDP/LThDP)} \quad (3)$$

$$\text{E−ThDP−substrate} \xrightarrow{k_3'} \text{carbanion/enamine (IndHEThDP}^-\text{/HBzThDP}^-\text{/HEThDP}^-\text{)} + CO_2 \quad (4)$$

$$\text{carbanion/enamine} + H^+ \xrightarrow{k_4'} \text{ThDP} + \text{product} \quad (5)$$

Please note that decarboxylation and product release (eqs 3 and 4, respectively) can be kinetically treated as being irreversible under the experimental conditions, whereas substrate binding (governed by k_2') can be assumed to be reversible. The net rate constant k_2' is then defined as

$$k_2' = \frac{k_2 k_3'}{k_{-2} + k_3'} \quad (6)$$

As the forward commitment factor c_f of substrate−ThDP decomposition

$$c_f = k_3/k_{-2} \quad (7)$$

in PDC and BFDC catalysis compounds has been estimated to be ≥5 (*22*−*24*), k_2' will mainly reflect the forward reaction of substrate binding. Although c_f remains to be determined for IPDC, we assume it to be in the first instance similar as in PDC and BFDC.

At substrate saturation, k_{cat} as a function of the forward rate constants of single steps is defined as

$$\frac{1}{k_{cat}} = \frac{1}{k_2'} + \frac{1}{k_3'} + \frac{1}{k_4'} \quad (8)$$

Under steady-state conditions and when [S] ≫ K_M, the formation and decomposition of all enzymatic intermediates are balanced.

Therefore, the relative intermediate concentrations can be directly correlated with the unimolecular forward (net) rate constants of their interconversions. The following correlations

hold true for IPDC catalysis at steady state:

$$\frac{[\text{substrate}-\text{ThDP}]}{[\text{ThDP}]} = \frac{k_2'}{k_3'} = a \quad (9)$$

$$\frac{[\text{product}-\text{ThDP}]}{[\text{substrate}-\text{ThDP}]} = \frac{k_3'}{k_4'} = b \quad (10)$$

The fraction of isolated cofactor as unsubstituted ThDP was corrected for nonsaturation of the enzyme with substrate according to the Michaelis−Menten equation.

Because of the nonenzymic decarboxylation of MThDP and IndLThDP after isolation, the observed relative intermediate concentrations were corrected for this decomposition, which can be treated as a first-order reaction (eq 11).

$$\frac{[\text{substrate}-\text{ThDP}]}{[\text{substrate}-\text{ThDP}]+[\text{product}-\text{ThDP}]}(t) = \frac{[\text{substrate}-\text{ThDP}]}{[\text{substrate}-\text{ThDP}]+[\text{product}-\text{ThDP}]}(t_0)e^{-kt} \quad (11)$$

The total of [product−ThDP] and [substrate−ThDP] can be considered to be constant:

$$[\text{substrate}-\text{ThDP}]+[\text{product}-\text{ThDP}] = [E_{as}] - [\text{ThDP}] \quad (12)$$

The corrected steady-state concentrations at t_0 after isolation are given as

$$[\text{substrate}-\text{ThDP}]_{corr}(t_0) = \frac{[\text{substrate}-\text{ThDP}]}{[\text{substrate}-\text{ThDP}]+[\text{product}-\text{ThDP}]}(t_0)([E_{as}] - [\text{ThDP}]) \quad (13)$$

$$[\text{product}-\text{ThDP}]_{corr}(t_0) = \left(1 - \frac{[\text{substrate}-\text{ThDP}]}{[\text{substrate}-\text{ThDP}]+[\text{product}-\text{ThDP}]}\right)(t_0)([E_{as}] - [\text{ThDP}]) \quad (14)$$

Using the experimentally determined and corrected steady-state intermediate distribution, k_{cat}, and eqs 8−10, the forward rate constants of single steps can be derived as follows:

$$k_2' = k_{cat}(1 + a + ab) \quad (15)$$

$$k_3' = k_{cat}\frac{(1 + a + ab)}{a} \quad (16)$$

$$k_4' = k_{cat}\frac{(1 + a + ab)}{ab} \quad (17)$$

Although there might still be some uncertainty with respect to the kinetic determinateness of k_2' (see above), any relative change in the distribution of the covalent substrate−ThDP and product−ThDP intermediates (b in eq 10) is indicative of an altered kinetic significance of the decarboxylation reaction (k_3') and product release (k_4'). Thus, mechanistic conclusions about the involvement of side chains in these elementary steps derived from the comparative intermediate analysis of the wild-type enzyme and active site variants seem to be justified.

Table 1: Steady-State Kinetic Properties of Wild-Type IPDC and Variants

protein	k_{cat}[a] (s^{-1})	K_M[a] (μM for Ipyr) (mM for BF/Pyr)	k_{cat}/K_M (s^{-1} mM^{-1})	K_i[b] (mM)
Ipyr				
wild type	0.98 ± 0.02	20 ± 1.3	49.0	−
Asp29Glu	nd[c]	−	−	−
Glu52Asp	0.10 ± 0.01	4.5 ± 1.4	22.2	−
His115Lys	0.31 ± 0.01	32.6 ± 4.1	9.5	−
Glu468Asp	0.040 ± 0.002	18.6 ± 2.9	2.2	−
Gln383Thr	2.05 ± 0.07	24.0 ± 2.7	85.4	−
BF				
wild type	11.6 ± 0.3	1.65 ± 0.03	7	−
Asp29Glu	0.010 ± 0.001	0.024 ± 0.003	0.4	−
Glu52Asp	0.87 ± 0.02	2.72 ± 0.18	0.3	−
His115Lys	0.29 ± 0.01	0.27 ± 0.02	1.1	−
Glu468Asp	0.07 ± 0.01	0.14 ± 0.01	0.5	−
Gln383Thr	2.25 ± 0.05	1.71 ± 0.14	1.3	−
Pyr				
wild type	0.88 ± 0.02	3.38 ± 0.18	0.25	164
Asp29Glu	0.019 ± 0.001	0.63 ± 0.10	0.03	61
Glu52Asp	0.060 ± 0.002	0.77 ± 0.10	0.08	71
His115Lys	0.016 ± 0.001	3.48 ± 0.33	0.004	141
Glu468Asp	0.069 ± 0.003	3.16 ± 0.32	0.02	247
Gln383Thr	2.06 ± 0.04	0.73 ± 0.06	2.82	9

[a] Catalytic constants were determined by employing a coupled NADH/ADH assay in 0.1 M MES buffer at pH 6.5 and 30 °C as described in ref *4*. [b] Substrate excess inhibition was exclusively observed for pyruvate turnover; inhibition constant K_i was calculated according to eq 1. [c] Not detectable.

The deprotonation rate constants of enzyme-bound ThDP were determined using a H−D exchange technique as described in ref *25*.

RESULTS AND DISCUSSION

IPDC mutants Asp29Glu, Glu52Asp, His115Lys, Gln383Thr, and Glu468Asp were successfully generated by site-directed mutagenesis of the wild-type gene. Expression and purification yields were as described for wild-type IPDC (*4*). Starting from 6 L of cultivation medium, we purified approximately 100 mg of IPDC to homogeneity by ammonium sulfate precipitation, size exclusion chromatography, and anion exchange chromatography.

Kinetic Constants of Wild-Type IPDC and Active Site Variants. The steady-state kinetic constants of wild-type IPDC and variants for turnover of substrates Ipyr, BF, and Pyr are summarized in Table 1, and examples of the direct v[S] plots for Glu468Asp are shown in Figure 3. All IPDC variants investigated so far exhibit significantly altered kinetic constants. In analogy to previous studies on other ThDP-dependent enzymes (*10*), we conservatively exchanged active site amino acids (Glu vs Asp and vice versa, His vs Lys). This conservative approach relying on differences in pK_a and distance allows light to be shed on the involvement of these residues in multiple steps of catalysis rather than completely abolishing activity, thereby complicating a complex assignment of these side chains with respect to overall catalysis.

A mutation of Asp29 located in the active cleft (compare panels A and B of Figure 1) to glutamate leads to an enzyme variant with the lowest specific activity of all the IPDC variants that were tested (Table 1). Whereas Pyr and BF are

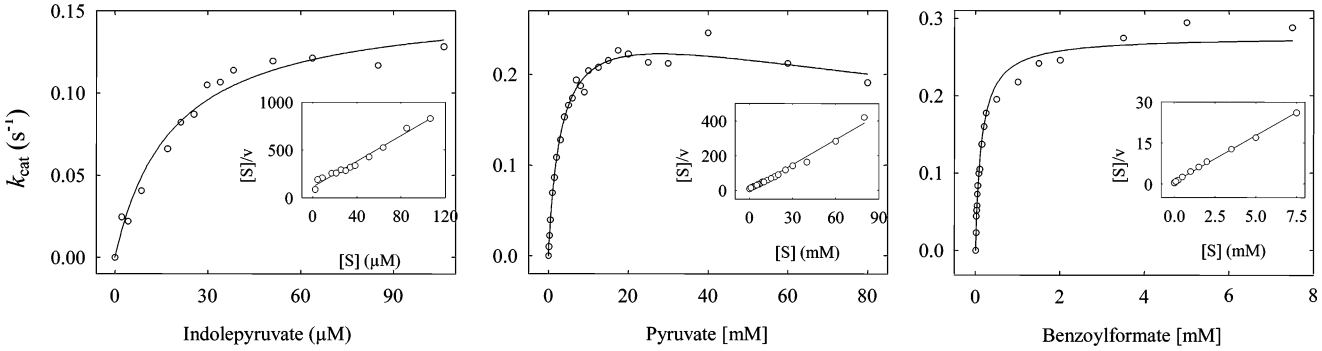

FIGURE 3: Dependence of the catalytic activity of IPDC Glu468Asp (relating to the tetramer) on the substrate concentration measured in 100 mM MES at pH 6.5 and 30 °C. The lines represent the fits to hyperbolic kinetics without (Ipyr and BF) and with (Pyr) substrate excess inhibition. The insets are Hanes plots.

still turned over by IPDC Asp29Glu, although with poor efficiency and rate, we could not detect any 3-indoleacetaldehyde formation when using Ipyr as a substrate. Instead of the typical A_{366} decrease related to the depletion of NADH in the coupled ADH/NADH assay (*4*), an increase in absorbance could be observed (see the section on Ipyr turnover), inviting speculation that this absorbance might correspond to a stable enzyme-bound intermediate. Proton NMR analysis confirmed that no indoleacetaldehyde is formed (data not shown). The apparent K_M value for BF and Pyr is lower than that of the wild-type enzyme; however, this may either reflect a higher substrate affinity (K_1) or, alternatively, an altered ratio of the net rate constants k_2', k_3', and k'_4, which also determine K_M. Using the minimal catalytic scheme given in eqs 2−5, K_M would be defined as

$$K_M = \frac{k_2'k_3'k_4' + k_{-1}k_3'k_4'}{k_1k_3'k_4' + k_1k_2'k_4' + k_1k_2'k_3'} \quad (18)$$

with

$$K_1 = k_{-1}/k_1 \quad (19)$$

A simple simulation demonstrates that, for instance, a specific reduction of k_4' by a factor of 10 would result in 4-fold reduction in the apparent K_M.

A Glu52Asp variant shows an approximate 10-fold reduction in overall activity for all three substrates that were employed (Table 1). If one keeps in mind that the conserved interaction between Glu52 and N1′ of ThDP (Figure 1A,B) triggers the reactivity of the 4′-amino group of the cofactor, this result implies that catalytic steps involving the aminopyrimidine proton relay are rate-determining for catalysis in the variant, independent of the chemical nature of the substrate to be converted.

There are striking differences in the kinetic behavior of a His115Lys variant concerning turnover of the different substrates. Whereas only a moderate 3-fold reduction in k_{cat} is observed for Ipyr conversion, effects are more distinct for BF (40-fold) and Pyr (50-fold) (Table 1). A comparison with the kinetic constants of the Asp29Glu variant demonstrates that Asp29 and His115 apparently constitute a functional dyad only for Pyr turnover. Since Asp29 and His115 are within hydrogen bonding distance of the X-ray structure (Figure 1A,B), we speculate that this pair of residues forms a proton relay that is involved in proton transfer steps during Pyr turnover. The catalytic roles of both residues for BF and Ipyr conversion do not seem to be in conjunction with regard to single microscopic steps. Remarkably, the His115Lys variant exhibits nearly identical k_{cat} values for BF and Ipyr.

Alongside His115 and Asp29, Glu468 is also perpendicular to the thiazolium ring of ThDP (Figure 1A,B) and might provide for acid/base chemistry in the course of catalysis. The overall catalytic constants of a Glu468Asp variant are nearly identical for the three different substrates that were converted (Table 1 and Figure 3). Unless these constants are coincidentially on the same order of magnitude, we might speculate that on a microscopic scale similiar events are rate-determining for catalysis, independent of the chemical nature of the substrate substituent.

In contrast to all other active center residues that were examined so far (Asp29, His115, Glu468, and Glu52), Gln383 is not capable of acting as an acid/base catalyst. If any, interactions on the basis of hydrogen bonds might orient the substrates and/or intermediates or in a more general rationalization by simple steric alignment. We replaced Gln383 with threonine, a less bulky residue that is the structural equivalent at this position in PDC (Figure 1A). The Gln383Thr variant of IPDC exhibits a 2-fold higher specific activity for Pyr conversion (Table 1), but remarkably, also the k_{cat} for the physiological substrate Ipyr is increased by the same factor. In contrast, BF is turned over slower than wild-type IPDC; in effect, IPDC Gln383Thr retains the high specificity for Ipyr, but the overall rate is balanced for the different substrates (Table 1). These findings have interesting mechanistic implications. Given that the rate preference for BF in wild-type IPDC is lost in the Gln383Thr variant, we suppose that Gln383 is a key determinant for the probable different binding/catalytic mode of BF on one hand and Pyr and Ipyr on the other.

Activation of ThDP in IPDC. It is now well accepted that the interaction between a highly conserved glutamate and N1′ of the aminopyrimidine ring of ThDP triggers the activation of the enzyme-bound cofactor, resulting in an acidification of the 4′-amino group of ThDP, possibly with discrete amounts of the 4′-imino form (*25*−*28*).

To kinetically relate the overall catalytic constants of wild-type IPDC and Glu52Asp to the ionization at C2, we determined the H−D exchange rate constants of these two enzymes at pH 6.5 according to the method of ref *25*. As a result, the observed H−D exchange rate constant of wild-type IPDC (k_{obs} = 70 ± 15 s^{-1}) exceeds that of Glu52Asp by more than 2 orders of magnitude (k_{obs} = 0.56 ± 0.11 s^{-1}). In wild-type IPDC, ionization at C2 is not rate-limiting

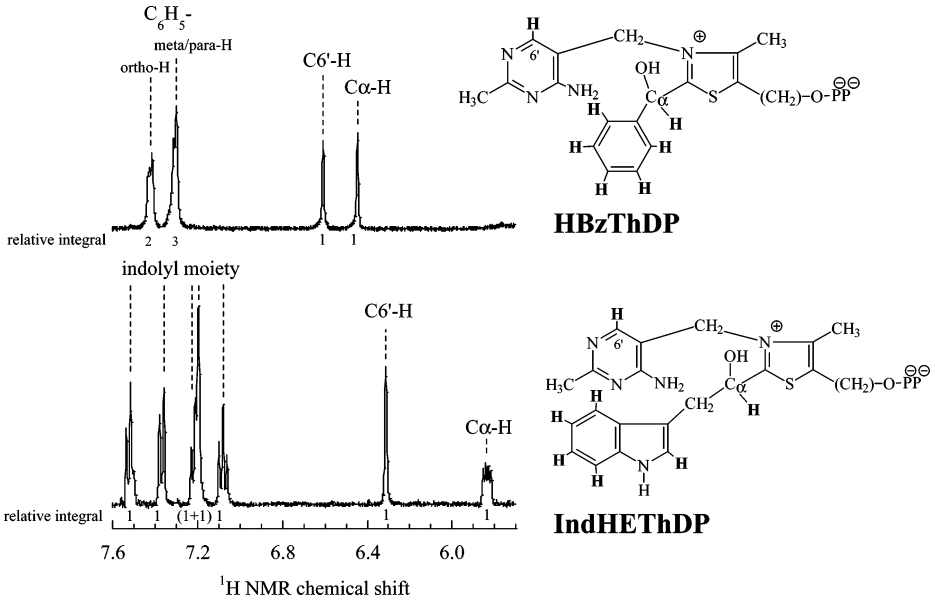

FIGURE 4: Chemical structures and low-field part of the ^{1}H NMR spectra of the tetrahedral product−ThDP adducts HBzThDP and IndHEThDP. ^{1}H NMR spectra were recorded in an aqueous solution containing 10% (v/v) D_2O at 25 °C and pH 0.75. The protons assigned in the spectra are indicated in boldface type in the chemical structures.

for turnover of all substrates (see Table 1). In Glu52Asp, however, this reaction appears to be partially rate-determining for catalysis when Ipyr and Pyr are converted. In contrast, k_{cat} for BF turnover [$k_{cat} = 0.9\ s^{-1}$ (Table 1)] is approximately 2 times larger than the observed rate constant of H−D exchange at C2 in this variant. It is implicit that k_{cat} must not exceed the rate constant of any elementary step of catalysis. However, it is important to realize that the H−D exchange technique is carried out in the absence of the substrate. Therefore, it provides a measure of the "per se functionality" of the cofactor proton relay in the ground state. Another important conclusion can be drawn from the fact that k_{cat} of IPDC Glu52Asp is lowered 10-fold when related to that of the wild-type enzyme, whereas the H−D exchange at C2 has been slowed by a factor of 100. This implies that the cofactor proton relay in the variant is also involved in rate-determining steps other than ionization at C2.

Intermediate Analysis. Standards and General Considerations. Recently, we have demonstrated that covalent intermediates invoked in thiamin diphosphate catalysis can be isolated by acid quench and analyzed by ^{1}H NMR spectroscopy (*10*, *29*).

Prior to the analysis of covalent intermediates transiently formed in the course of nonoxidative decarboxylation of Ipyr and BF by IPDC, we synthesized the tetrahedral product−ThDP adducts HBzThDP and IndHEThDP as standards (see Materials and Methods and Figure 4) and studied their spectroscopic properties and stability under the acidic conditions that are employed for isolation and analysis. The ^{1}H NMR spin systems are consistent with the chemical structures of HBzThDP and IndHEThDP, the low-field part of the ^{1}H NMR spectra of both compounds covering the aromatic substrate-derived protons (benzyl or indolyl moiety); the C6′-H resonance of the aminopyrimidine ring of ThDP and the C_α-H resonance are given in Figure 4. Most notably, this is the first direct observation of any covalent indolyl−ThDP adduct. The C6′-H signals of both intermediates are not obscured by signals of substrates or products and may therefore be used as a quantitative measure. So far, any attempt to chemically synthesize the tetrahedral substrate−ThDP adducts MThDP (R. Kluger, personal communication) and IndLThDP (instability of the reactant Ipyr) were unsuccessful, but the synthesis and chemical properties of 2-mandelylthiamin (MTh) have been recently reported by Kluger's group (*30*, *31*) and gave an indication of an extremely low pK_a for the carboxyl group of MTh (p$K_a = 0.2$) and a $t_{1/2}$ of decarboxylation for the carboxylate form of ∼45 min. Considering that the pK_a of MThDP is the same as that of MTh, MThDP will lose CO_2 under the conditions that are used for isolation and NMR analysis (pH 0.75).

Intermediate Analysis Using the Substrate Pyr. When Pyr is converted to acetaldehyde by IPDC, the covalent intermediates LThDP and HEThDP (representing the carbanion/enamine and its conjugate acid) can be detected by ^{1}H NMR. In wild-type IPDC, only ThDP and HEThDP can be isolated in the steady state at substrate saturation (Figure 5), implying the formation of LThDP (step 2 in Figure 2) and product release (steps 4a and 4b in Figure 2) are partially rate-determining for overall catalysis (Table 1). The nonobservation of LThDP indicates that the decarboxylation of the latter (step 3 in Figure 2) is significantly faster than step 4 and, a similar forward commitment of LThDP decomposition provided as observed in PDC and BFDC catalysis, also step 2.

To assign functional roles of active site residues to distinct catalytic steps, the steady-state intermediate distribution of various mutant proteins has been analyzed (Figure 5). In summary, all variants exhibit specific deficiencies, which can be attributed to either the formation of LThDP, its decarboxylation, or acetaldehyde liberation (Table 2). Glu468 and Glu52 are important for an efficient ligation of pyruvate to the ThDP ylide, and the respective Asp variants show an approximate 10-fold reduction in the rate constant of this step of catalysis. The decarboxylation of LThDP is assisted by Glu468 and His115 as evidenced by its accumulation in the steady state of Glu468Asp and His115Lys only, and by significantly decreased *b* values (see eq 10). The rate constant of decarboxylation in these IPDC variants is approximately

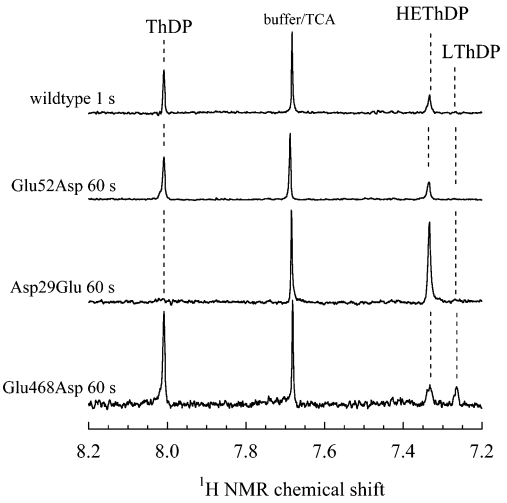

FIGURE 5: Steady-state intermediate distribution of covalent intermediates in the nonoxidative decarboxylation of pyruvate (see Figure 2) by wild-type IPDC and selected enzyme variants (Glu52Asp, Asp29Glu, and Glu468Asp) at substrate saturation (50 mM pyruvate). The intermediates were isolated by acid quench after a reaction time of either 1 s (wild type) or 60 s (variants) in 0.1 M MES at pH 6.5 and 30 °C and analyzed by ^{1}H NMR at pH 0.75 using the characteristic C6′-H chemical shifts (*10*).

2 orders of magnitude smaller than in the wild-type enzyme. The liberation of acetaldehyde is dependent on the concerted action of an Asp29-His115 dyad and the Glu52−cofactor shuttle. Interestingly, the formation of LThDP is specifically accelerated in the "pseudo-PDC" Gln383Thr variant. On the basis of the functional assignment and the X-ray crystallography structure of the parental enzyme, we suggest that the carboxylate of the substrate/LThDP makes contact with the side chains Glu468 and His115, leading to a perpendicular orientation with respect to the thiazolium ring (Figure 6). The intriguing observation that Glu52 as the chemical trigger of the 4′-amino group of the cofactor is mandatory for both substrate binding and product release favors an (*S*)-configuration of the tetrahedral LThDP intermediate. Thus, the 4′-amino/imino function of the cofactor would be in the vicinity of the α-hydroxyl group and may be involved in the protonation of the substrate carbonyl (substrate binding) and the ionization of the α-hydroxyl function (acetaldehyde release). The putative (*S*)-configuration of LThDP would also result in the spatial proximity of the substrate-derived methyl and the side chain of Gln383, being in accord with the observed altered substrate specificity in the Gln383 variant (Table 1). After the decarboxylation of LThDP, the resultant carbanion/enamine is protonated, facilitating the ionization of the hydroxyl function and breakdown of the C2−C_α bond. As mentioned above, the 4′-amino (imino) group of the cofactor is likely involved in the protonation or deprotonation of the alkoxidic oxygen or hydroxyl group, respectively. Therefore, we propose that the Asp29-His115 dyad, which is exclusively conserved in the class of decarboxylases, catalyzes the protonation of the carbanion/enamine (Figure 6). Although the carbanion and enamine are said to be mesomeric, they must be regarded as different chemical species in the enzyme-bound state; the hybridization of C_α will be either sp^3 (carbanion) or sp^2 (enamine). To facilitate protonation, it would be more reasonable to retain the sp^3 hybridization at C_α after decarboxylation of LThDP (or to transfer the proton late in the same transition state) rather than involving two inverse hybridization steps. On the other hand, model studies suggest a more neutral transition state of decarboxylation (resembling the uncharged enamine/CO_2 pair) with considerable delocalization of the electron pair since a large decrease in the activation barrier has been observed in less polar solvents as a consequence of the greater destabilization of the dipolar reactant state (*12*, *32*, *33*).

Intermediate Analysis Using the Substrate BF. When wild-type IPDC is reacted with BF, no intermediates other than ThDP and HBzThDP could be isolated at steady state and substrate saturation (data not shown), pointing to a rate-determining ligation of BF to the ThDP ylide (step 2 in Figure 2) and benzaldehyde release (step 4 in Figure 2) (Table 3). We could not isolate MThDP from the parental enzyme; however, in some IPDC variants, such as Asp29Glu, His115Lys, and Glu468Asp, we obtained strong evidence for its occurrence and accumulation in the steady state implying an impaired decarboxylation in these variants. As shown for IPDC Asp29Glu in Figure 7, ThDP, HBzThDP, and a new ThDP intermediate can be isolated at steady state using the C6′-H resonances. This intermediate can be detected only shortly after isolation (Figure 7A). In the course of NMR data acquisition (usually 4−6 h), it decays quantitatively to HBzThDP (Figure 7B). The ^{1}H NMR spin system of MThDP is nearly identical compared to that of HBzThDP, except that the C_α-H resonance is missing. Since the observed first-order rate constant ($k_{obs} = 3.1 \times 10^{-4}$ s^{-1} at 25 °C) of its decay (Figure 7C) is in good agreement with that reported for the decarboxylation of MTh (*30*), we conclude that this new intermediate can be indeed termed MThDP. Because of the intrinsic instability of MThDP (loss of CO_2), the observed relative intermediate concentrations need to be corrected for the nonenzymic decomposition after isolation according to eqs 11−14. The corrected intermediate distribution may then be used to calculate reliable rate constants of microscopic steps of catalysis. It must be noted that MThDP will be detected in a quantitative manner only, if its persistent steady-state concentration is ≥20% of the active site concentration.

An analysis of the steady-state intermediate distribution of several IPDC variants and resultant net rate constants revealed defined deficiencies (Table 3) that in part coincide with our observations about the intermediate distribution during turnover of Pyr (Table 2). Formation of the tetrahedral substrate−ThDP adduct MThDP is mediated both by the Glu-Asp-His triad enfolding the thiazolium nucleus of ThDP and the cofactor−Glu52 proton shuttle (compare panels A and B of Figure 1). The decarboxylation of MThDP is strictly dependent on the functionality of the Glu468-Asp29-His115 motif, and a mutation of any of these side chains slows the decarboxylation reaction by several orders of magnitude (Table 3). Product release, however, is only significantly affected in the Asp29Glu mutein; other variants exhibit only minor effects. A rationalization of these findings in mechanistic terms further buttresses our suggested model of catalysis deduced from the intermediate studies on pyruvate turnover. It is evident that the carboxylate of BF and MThDP will likely make "productive contact(s)" with the side chains of the Glu-Asp-His motif, which appears to form a substrate substituent-independent "carboxylate pocket", as already suggested for Pyr−LThDP (Figure 5). It is more difficult to

Table 2: Net Rate Constants of Elementary Catalytic Steps of Nonoxidative Decarboxylation of Pyr by IPDC

	overall activity		C−C bonding pyruvate and C2 ylide[a]		decarboxylation of LThDP[a]		product release[a]	
protein	k_{cat} (s^{-1})	$R(k_{cat})$[b]	k_2' (s^{-1})	$R(k_2')$[b]	k_3' (s^{-1})	$R(k_3')$[b]	k_4' (s^{-1})	$R(k_4')$[b]
wild type	0.88	−	1.25	−	≥19.05	−	3.46	−
Asp29Glu	0.019	46	≥0.31	≤4	≥0.31	−	0.02	173
Glu52Asp	0.057	15	0.10	13	≥1.21	−	0.16	22
His115Lys	0.016	55	≥0.27	≤4	0.14	≥136	0.02	173
Glu468Asp	0.069	13	0.11	11	0.34	≥56	0.35	10
Gln383Thr	2.05	$(2.3)^{-1}$	6.51	$(5.2)^{-1}$	≥40.72	−	3.24	1

[a] First-order net rate constants of covalent pyruvate binding to ThDP (k_2'), decarboxylation of LThDP (k_3'), and release of acetaldehyde from HEThDP (k_4') were calculated from the steady-state intermediate distribution analyzed by ^{1}H NMR and k_{cat} according to eqs 8−10 and 15−17. When the peak corresponding to a given intermediate could not be resolved, lower limits for the net rate constant for its breakdown were calculated from the upper limit of the peak area, defined as a hypothetical peak height of 3 times the signal-to-noise ratio. The major source of error of all rate constants given in this table is based on the computer-assisted integration of the intermediate signals, depends on the signal-to-noise ratio of the individual signals, and was found to be not larger than 10−15%. [b] Factor R is defined as the ratio of the rate constant calculated for wild-type IPDC divided by that of the respective variant [i.e., $R(k_{cat}) = k_{cat}^{wt}/k_{cat}^{variant}$].

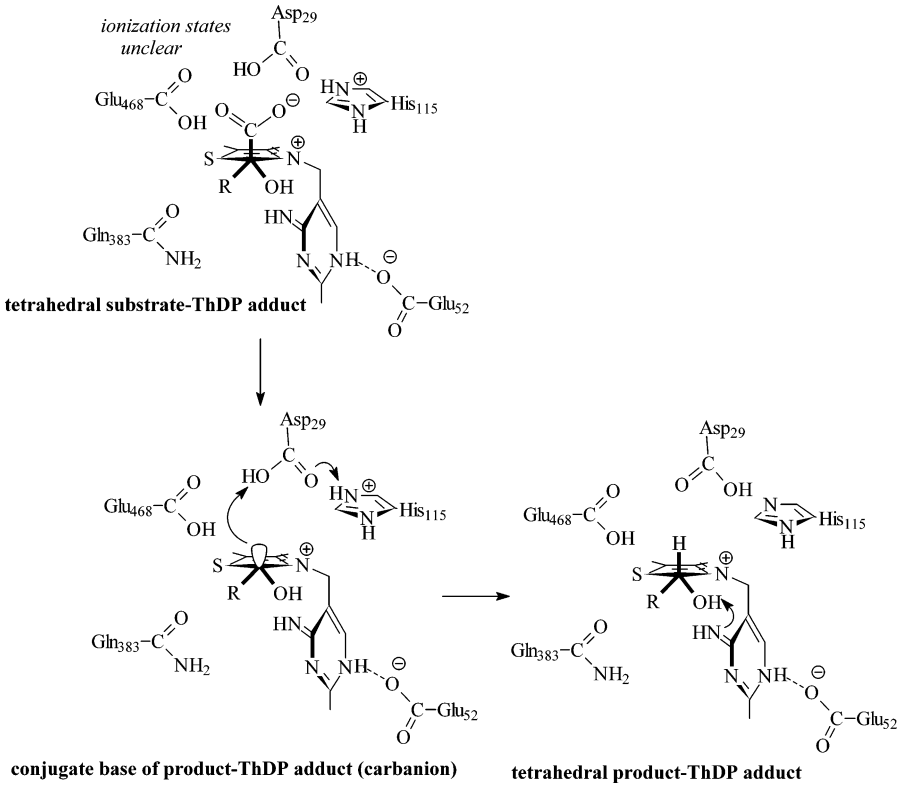

FIGURE 6: Putative spatial orientation of key intermediates in the course of nonoxidative decarboxylation of α-ketoacids by IPDC (see the text). The proposed conformations of the intermediates and resultant interactions with active site residues are consistent with specific kinetic deficiencies of active site single variants detected by ^{1}H NMR-based intermediate analysis (Tables 2−4).

microscopically decipher the product release step. Although Asp29 is most crucial and probably involved in a proton transfer step in the course of product release, we cannot dissect by our NMR method whether protonation of the carbanion or ionization of the α-hydroxyl group is affected in the Asp29Glu variant. We speculate on the basis of our studies about pyruvate turnover and the X-ray crystallography structure of IPDC Asp29 being involved in the protonation of the carbanion. If protonation of the carbanion is abolished or slowed, a low-energy enamine species with considerable conjugation of the benzyl moiety of the substrate and the thiazolium ring of the cofactor may form and, thus, result in a tremendous pK_a (C_α-H) suppression in a low-polarity microenvironment (*21*). Paraphrased, the protonation step of a stabilized intermediate (the enamine) might be more critical than ionization of a kinetically labile α-hydroxyl function. The summarized net rate constants of wild-type IPDC and variants acting on BF show that contrary to the observations on Pyr turnover no residue other than Asp29 is kinetically critical for product release. We tentatively assigned the 4′-imino group of the cofactor to accept the proton of the hydroxyl group of HEThDP as evidenced by a slow product release in the Glu52Asp variant. If ionization of the α-hydroxyl group would be indeed partially rate-determining for product release, our results on BF conversion in Glu52Asp are somewhat surprising, since the only slightly different pK_a of the α-OH of HEThDP and HBzThDP will not explain the large kinetic difference in acetaldehyde or benzaldehyde release in the variant. Noteworthy also in the wild-type enzyme is the fact that benzaldehyde release is approximately 10 times faster than that of acetaldehyde (Tables 2 and 3). This intriguing observation implies a step other than ionization of the α-OH is rate-determining for product release, probably the cleavage of the carbon−carbon bond between

Table 3: Net Rate Constants of Elementary Catalytic Steps of Nonoxidative Decarboxylation of Benzoylformate (BF) by IPDC

	overall activity		C−C bonding BF and C2 ylide[a]		decarboxylation of MThDP[a]		product release[a]	
protein	k_{cat} (s^{-1})	$R(k_{cat})$[b]	k_2' (s^{-1})	$R(k_2')$[b]	k_3' (s^{-1})	$R(k_3')$[b]	k_4' (s^{-1})	$R(k_4')$[b]
wild type	11.60	−	18.45	−	≥92.50	−	37.10	−
Asp29Glu	0.010	1160	0.017	1085	0.025	≥3700	0.10	371
Glu52Asp	1.16	10	1.27	15	≥38.25	−	19.05	2
His115Lys	0.28	41	0.58	32	0.70	≥132	2.90	13
Glu468Asp	0.07	166	0.10	184	0.26	≥356	2.25	16
Gln383Thr	2.25	5	2.85	6	≥49.75	−	13.50	3
wild-type CH_3O-BF	0.87	13	1.50	12	2.32	≥40	≥21.05	≤1.8
wild-type Br-BF	0.80	14	2.12	9	≥6.50	−	1.60	23

[a] First-order net rate constants of covalent benzoylformate binding to ThDP (k_2'), decarboxylation of MThDP (k_3'), and release of benzaldehyde from HBzThDP (k_4') were calculated from the steady-state intermediate distribution analyzed by ^{1}H NMR and k_{cat} according to eqs 8−10 and 15−17. The intermediate distribution was corrected for the nonenzymic decarboxylation of MThDP after isolation according to eqs 11−14. When the peak corresponding to a given intermediate could not be resolved, lower limits for the net rate constant for its breakdown were calculated from the upper limit of the peak area, defined as a hypothetical peak height of 3 times the signal-to-noise ratio. The major source of error of all rate constants given in this table is based on the computer-assisted integration of the intermediate signals, depends on the signal-to-noise ratio of the individual signals, and was found to be not larger than 10−15%. [b] Factor R is defined as the ratio of the rate constant calculated for wild-type IPDC divided by that of the respective variant [i.e., $R(k_{cat}) = k_{cat}^{wt}/k_{cat}^{variant}$].

ThDP and substrate-derived C_α. In the transition state of this step, a carbocation/carbanion pair is formed prior to rehybridization of the C_α to the carbonyl (Figure 8). Apparently, a benzyl substituent could more effectively compensate for the positive charge than a methyl group and, thus, explain the lower activation barrier of benzaldehyde release.

Intermediate Analysis during Turnover of Para-Substituted BF and Mechanistic Implications for the Transition States of Carbonyl Addition/Elimination and Decarboxylation. For a more detailed analysis of the rate dependence of microscopic steps of catalysis on the electronic properties of the substrate substituent, we studied the steady-state intermediate distribution during turnover of selected para-substituted benzoylformates. We have demonstrated recently that both electron-donating and electron-withdrawing para substituents of BF lead to inversely directed changes in the rate-determining step(s) in IPDC catalysis (*4*). In a first approach, we analyzed the steady-state intermediate distribution of *p*-methoxy-BF (*p*-CH_3O-BF) and *p*-bromo-BF (*p*-Br-BF) conversion; both alternative substrates are turned over by IPDC with approximately $^1/_{10}$ of the overall rate constant of unsubstituted BF. The chemical shifts of the ^{1}H NMR resonances of the isolated ThDP adducts differ only slightly from those of MThDP and HBzThDP (data not shown). While using *p*-Br-BF as a substrate, we isolated comparable fractions of ThDP and *p*-Br-HBzThDP in the steady state. On the other hand, ThDP and *p*-CH_3O-MThDP were isolated under steady-state conditions during *p*-CH_3O-BF turnover. As previously observed for MThDP, *p*-CH_3O-MThDP decays quantitatively to *p*-CH_3O-HBzThDP after isolation with a first-order rate constant of 1.6×10^{-4} s^{-1}. The calculated net rate constants of elementary steps (Table 3) demonstrate the inversely directed effects of the para substituents on the rate dependence on decarboxylation in comparison to that of unsubstitued BF. Clearly, decarboxylation of the tetrahedral substrate−ThDP adduct becomes rate-determining when the electron-donating methoxy function replaces H in the para position. A substitution with the electron-withdrawing Br leads to the slower formation of the tetrahedral substrate adduct and a slower product release step, whereas no apparent effect could be detected for the decarboxylation step. In mechanistic terms, several conclusions can be drawn from these observations. The destabilizing effect of the electron-donating *p*-CH_3O function upon the decarboxylation step suggests a carbanion-like transition state. Alternatively, the tetrahedral substrate−ThDP adduct may be stabilized, thus resulting in a higher activation barrier for the decarboxylation step. In contrast, the first-order rate constant of decarboxylation of *p*-Br-MThDP in IPDC is significantly higher (Table 3) and demonstrates that the substrate R substituent not only is a "spectator" of the decarboxylation with the thiazolium nucleus as the major electron sink but also contributes to the stabilization or destabilization of the α-carbanion or carbanion-like transition state, respectively, by its intrinsic electronic properties. The product release step which presumably involves a carbocation/carbanion pair in its reaction sequence (Figure 8) is also sensitive to the para substituent but oppositely directed as the decarboxylation reaction. Here, the electron-donating *p*-CH_3O may more effectively stabilize the positive charge of the carbocation in the transition state than the electron-withdrawing *p*-Br function does. Our studies are in accord with investigations of Kenyon, Cook, and co-workers, who used ^{13}C and solvent deuterium isotope effects to conduct linear free energy relationship studies on BFDC catalysis (*24*).

Abortive Side Reactions of HBzThDP$^-$ in IPDC? We address an important point regarding abortive side reactions of central catalytic intermediates. Kluger and co-workers demonstrated in model studies that the carbanion/enamine form of HBzThDP is subject to an irreversible fragmentation reaction yielding dimethylaminopyrimidine and a phenyl thiazoldiphosphate ketone, a reaction that competes with the protonation (*31*). Neither in the wild-type protein nor in the variants investigated did we obtain evidence for this side reaction; only ThDP, MThDP, and HBzThDP could be isolated as intermediates (even after prolonged reaction times), thus supporting Kluger's suggestion (*34*) of a stereoelectronic control of the conversion of HBzThDP$^-$ (data not shown).

Intermediate Analysis Using the Substrate Ipyr. In analogy to our studies on covalent intermediates deriving from the reaction of IPDC with Pyr and BF, we analyzed the intermediate distribution during Ipyr conversion at different reaction times (0−2000 ms) and at substrate saturation to ensure true steady-state conditions. Because of the poor solubility of Ipyr in aqueous buffer ($c_{max} \approx 5$ mM) and the

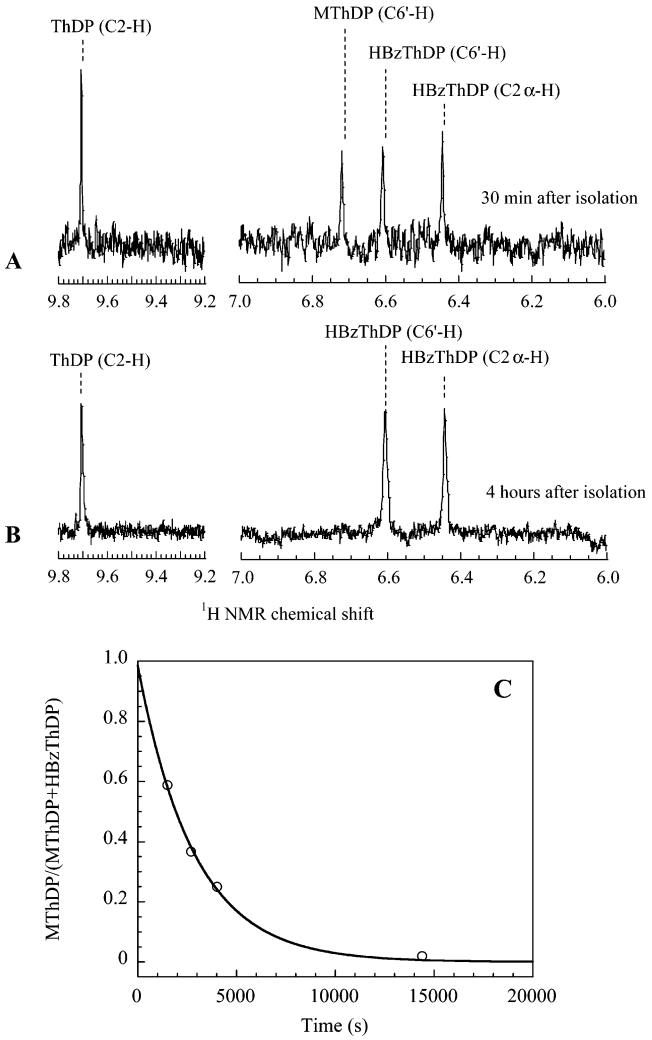

FIGURE 7: Quantification of covalent intermediates in the nonoxidative decarboxylation of benzoylformate (see Figure 2) by IPDC variant Asp29Glu. The intermediates were isolated by acid quench after a reaction time of 60 s in 0.2 M MES at pH 6.5 and 30 °C and analyzed by ^{1}H NMR at pH 0.75 using the C6′-H chemical shifts of HBzThDP and MThDP, and the C2-H chemical shift of ThDP (see the text). (A) Downfield section of the ^{1}H NMR spectrum after an acquisition time of 30 min. (B) Downfield section of the ^{1}H NMR spectrum after an acquisition time of 4 h. (C) Reaction kinetics of decarboxylation of isolated MThDP at pH 0.75 and 25 °C. The line represents a fit to a monoexponential function given in eq 11 and yielded a first-order rate constant of 3.1×10^{-4} s^{-1}.

high enzyme concentration needed for the NMR analysis, most of the substrate is converted within a couple of seconds in the wild-type enzyme, thus limiting true steady-state conditions to the millisecond time scale.

As already observed for Pyr and BF turnover, only the covalent product−ThDP adduct IndHEThDP and ThDP can be detected in the steady state of the wild-type enzyme (data not shown), demonstrating that (i) the formation of the tetrahedral substrate−ThDP adduct and product release are partially rate-determining and (ii) the decarboxylation of IndLThDP is significantly faster (Table 4). However, there is a possible drawback of the isolation and analysis procedure. The absence of IndLThDP in the ^{1}H NMR spectra might not neccessarily reflect a low kinetic significance of the decarboxylation step, but may result from a fast decarboxylation of the intermediate after its isolation. A detailed intermediate analysis of some IPDC variants, such as Glu468Asp, showed that IndLThDP can indeed be isolated, although it decarboxylates quantitatively to IndHEThDP with a k_{obs} of 2×10^{-4} s^{-1} at 25 °C and pH 0.75 (Figure 9). The ^{1}H NMR spin system of IndLThDP is identical to that of IndHEThDP except the missing C_α-H resonance. As depicted in Figure 9A, the C6′-H singlet can be used to discriminate IndLThDP and IndHEThDP quantitatively.

The intermediate distribution was corrected for the nonenzymic decarboxylation of IndLThDP according to eqs 11−14. The calculated net rate constants of wild-type IPDC and variants are summarized in Table 4 and reveal distinct deficiencies in the different variants that overlap with our results on BF and Pyr turnover. In the section on steady-state kinetics, we have already reported on the absolute inability of the Asp29Glu variant to release the reaction product 3-indoleacetaldehyde. Above, we have also reported on the unexpected increase in absorbance at A_{366} in the coupled ADH/NADH assay. The UV−vis absorbance spectrum of IPDC Asp29Glu reacting with Ipyr in the absence of ADH and NADH shows a new absorbance band at 380 nm (Figure 10A). The intermediate analysis of this variant reveals that product release is abolished because only IndHEThDP can be isolated (Figure 10 inset). After acid quench separation of IndHEThDP from the enzyme and readjustment of the pH from 0.75 to 6.5, no absorbance in the spectral region is observed for the isolated compound. This result invites speculation that the absorbance at 380 nm is caused by the enamine/carbanion form of IndHEThDP in the active site as a highly conjugated system. Similar observations were made in BFDC; here, a species with an absorption maximum of 400 nm was assigned to the enamine/carbanion form of *p*-NO_2-HBzThDP (*8*). The results for the IPDC Asp29Glu variant imply that the protonation of the carbanion/enamine of IndHEThDP is disturbed. This finding coincides with our observations on Pyr and BF turnover (see the respective sections). Remarkably, the enamine in Asp29Glu appears to be stabilized in the active site. Assuming the pK_a of C2α-H of free IndHEThDP is in the range of those of HBzThDP [pK_a = 15.4 (*21*)] and HEThDP (pK_a ≈ 18−20), the enzyme environment must suppress the pK_a by several orders of magnitude, probably via a very low effective dielectric constant in the active site. A similar observation has been made while HBzThDP was partitioned on apo-PDC (*21*). The kinetic characterization of all other IPDC variants by the NMR intermediate analysis revealed that functional groups of active site side chains and of the cofactor are involved in similar steps of catalysis during turnover of the three different substrates (Table 4). Therefore, we conclude that the conformation of the key intermediates in the active site of IPDC is conserved: the substrate−carboxylate compound is accommodated in the Glu-Asp-His pocket, the carbonyl-derived oxygen is in the vicinity to the 4′-imino/amino group of the cofactor, and Gln383 is a main element of the substrate specificity pocket.

CONCLUSIONS

Although high-resolution structures of many ThDP enzymes have been determined (*7*, *35*−*41*), only few intermediates could be analyzed structurally, including an oxyethyl radical in pyruvate:ferredoxin oxidoreductase (*42*) and the

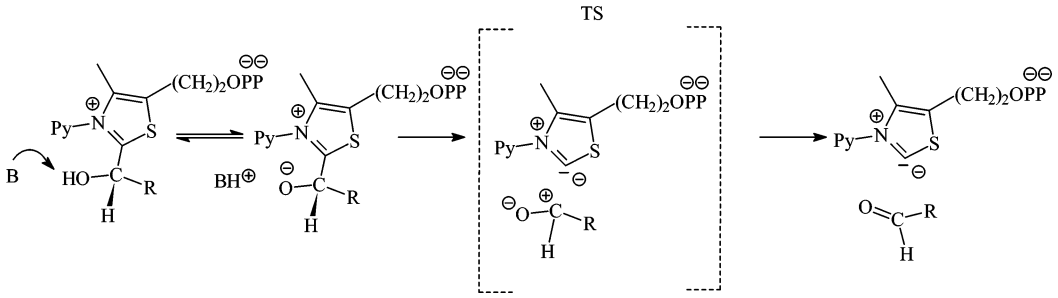

FIGURE 8: Reaction sequence of product release in nonoxidative decarboxylation of α-ketoacids by IPDC and the putative relevant transition state.

Table 4: Net Rate Constants of Elementary Catalytic Steps of Nonoxidative Decarboxylation of 3-Indolepyruvate (Ipyr) by IPDC

	overall activity		C−C bonding Ipyr and C2 ylide[a]		decarboxylation of IndLThDP[a]		product release[a]	
protein	k_{cat} (s^{-1})	$R(k_{cat})$[b]	k_2' (s^{-1})	$R(k_2')$[b]	k_3' (s^{-1})	$R(k_3')$[b]	k_4' (s^{-1})	$R(k_4')$[b]
wild type	0.97	−	2.17	−	≥7.50	−	2.30	−
Asp29Glu	nd[c]	−	−	−	−	−	rate-determining	−
Glu52Asp	0.10	10	0.14	15	≥1.37	−	0.55	4
His115Lys	0.31	3	0.65	3	≥4.00	−	0.67	3
Glu468Asp	0.037	26	0.055	40	0.20	≥38	0.25	9
Gln383Thr	2.05	$(2)^{-1}$	8.60	$(4)^{-1}$	4.75	≥2	6.15	$(2.7)^{-1}$

[a] First-order net rate constants of covalent 3-indolepyruvate binding to ThDP (k_2'), decarboxylation of IndLThDP (k_3'), and release of 3-indoleacetaldehyde from IndHEThDP (k_4') were calculated from the steady-state intermediate distribution analyzed by ^{1}H NMR and k_{cat} according to eqs 8−10 and 15−17. The intermediate distribution was corrected for the nonenzymic decarboxylation of IndLThDP after isolation according to eqs 11−14. When the peak corresponding to a given intermediate could not be resolved, lower limits for the net rate constant for its breakdown were calculated from the upper limit of the peak area, defined as a hypothetical peak height of 3 times the signal-to-noise ratio. The major source of error of all rate constants given in this table is based on the computer-assisted integration of the intermediate signals, depends on the signal-to-noise ratio of the individual signals, and was found to be not larger than 10−15%. [b] Factor R is defined as the ratio of the rate constant calculated for wild-type IPDC divided by that of the respective variant [i.e., $R(k_{cat}) = k_{cat}^{wt}/k_{cat}^{variant}$]. [c] Not detectable. Under the experimental conditions, no 3-indoleacetaldehyde could be detected utilizing the coupled ADH/NADH assay according to ref *4* or by ^{1}H NMR spectroscopy.

carbanion/enamine in transketolase (*43*). From a kinetic point of view, the formation and decomposition of an exclusive subset of intermediates with appropriate spectroscopic properties, such as radical intermediates or the elusive enamine, have been analyzed by ESR, circular dichroism, and time-resolved spectroscopy, but the analysis was mainly restricted to single events in catalysis (electron transfer in POX and PFOR), the use of nonphysiological substrates with improved spectroscopic properties (*p*-nitro-BF in BFDC), and an assignment of signals based on model studies with no ultimate proof for the enzymic system (*8*, *9*, *44*−*46*). A comparative intermediate analysis of wild-type IPDC and variants reacting with the alternative substrates Ipyr, BF, selected para-substituted BFs, and Pyr by the quench/NMR method not only confirms the generality of Breslow's mechanism but also may be used together with steady-state kinetics as a valuable tool for mechanistically deciphering microscopic steps of catalysis and mapping interactions of the different intermediates with active site side chains. Although it is not the purpose of this research report to review the current mechanistic understanding of ThDP enzymes (excellent reviews on this subject are given in refs *12* and *33*), we discuss our results in the context of relevant model studies and, if available, enzymic systems.

Proton Management by an Enzyme−*Cofactor Proton Shuttle.* First, both the thiazolium ring and the aminopyrimidine nucleus of ThDP are involved in enzymic catalysis, thus constituting a dual catalytic apparatus. In IPDC Glu52Asp, several steps of catalysis are abolished, including the generation of the reactive ylide species, formation of the substrate−ThDP adduct, and aldehyde release (Tables 2−4). Since the Glu52−N1′ interaction is thought to activate the protein−cofactor proton shuttle, it is reasonable to assume that the exocyclic 4′-amino group of ThDP participates in various steps of enzymic catalysis, either as a proton donor (amino form)/acceptor (imino form) or in terms of orienting intermediates through hydrogen bonding. Recently, Jordan and co-workers accumulated evidence that the 1′,4′-imino tautomer indeed forms in the active site of various ThDP enzymes and is the predominant species in the intermediates LThDP and HEThDP. In contrast, the 4′-amino tautomer could be detected in the Michaelis complex (*27*, *28*). These results and the NMR intermediate studies on *Zm*PDC (*10*) and IPDC (this study) clearly suggest a catalytic role of the aminopyrimidine ring in multiple proton transfer steps. H−D exchange experiments with several members of the ThDP enzyme family revealed that the 4′-imino group abstracts the C2 proton, thereby generating the reactive ylide form of the cofactor (*25*, *26*). The intriguing observation of a slowed substrate ligation and product release in less reactive "4′-amino variants" with substitutions of the conserved glutamate (ref *10* and this study) tempts us to conclude that the proton shuttle is functionally involved in the carbonyl addition−elimination reaction in terms of protonation of the carbonyl oxgen and deprotonation of the α-OH of the product−ThDP adduct as a general feature in enzymic ThDP catalysis according to the least-base principle. Evidently, all reactions catalyzed by ThDP enzymes involve ylide generation and carbonyl addition/elimination so that a common catalytic apparatus, i.e., the enzyme-bound and activated cofactor itself, appears to be more structurally suited to meet the catalytic challenges of this common reaction type than catalysis by enzyme side chains. This hypothesis is further buttressed by structural analysis of intermediates in various

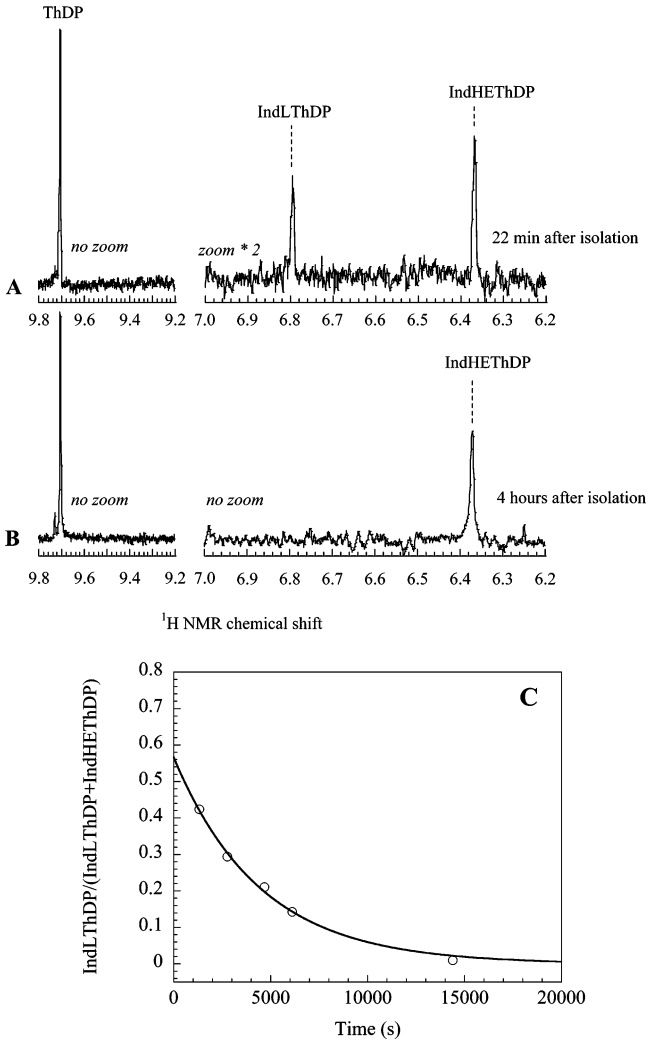

FIGURE 9: Quantification of covalent intermediates in the nonoxidative decarboxylation of 3-indolepyruvate (see Figure 2) by IPDC variant Glu468Asp. The intermediates were isolated by acid quench after a reaction time of 60 s in 0.2 M MES at pH 6.5 and 30 °C and analyzed by ^{1}H NMR at pH 0.75 using the C6′-H chemical shifts of IndHETHDP and IndLThDP, and the C2-H chemical shift of ThDP (see the text). (A) Downfield section of the ^{1}H NMR spectrum after an acquisition time of 22 min. (B) Downfield section of the ^{1}H NMR spectrum after an acquisition time of 4 h. (C) Reaction kinetics of decarboxylation of isolated IndLThDP at pH 0.75 and 25 °C. The line represents a fit to a monoexponential function (eq 11) and yielded a first-order rate constant of 2×10^{-4} s^{-1}.

enzymes. In transketolase (*43*), branched chain α-ketoacid dehydrogenase (*49*), and pyruvate oxidase (*50*), the elusive enamine/carbanion intermediate adopts a conformation in which the substrate carbonyl-derived α-OH is positioned in the vicinity to the 4′-amino (imino) group of the aminopyrimidine ring, thus favoring an intramolecular proton transfer. We may speculate that by considering the rule of microscopic reversibility a similar situation may hold true for the reverse type of reaction, the carbonyl addition of the substrates or products. In BFDC, the unreactive substrate analogue (*R*)-mandelate is bound in a way that the hydroxyl group (the carbonyl equivalent) is within hydrogen bonding distance of the 4′-amino group and a histidine side chain (*9*). Model studies could not evidence a participation of the amino group in proton transfer steps (*51*), but it is difficult to establish model systems that match or resemble the conditions in the active sites. First and foremost, the enzyme-bound cofactor adopts the enforced *V* conformation, which fixes the 4′-amino/imino group in the vicinity of C2-H, presumably resulting in a high effective molarity. Second, the cofactor is activated by the Glu−N1′ interaction and was shown to form a potent 4′-imino base even under physiological conditions. Third, solvent sequestration from the active site during catalysis (closed transition states) may help to favor "productive" reactions [e.g., the ligation of the C2 carbanion with the carbonyl substrate vs solvent-mediated reprotonation (*33*)].

Stereochemical Control of Decarboxylation. Aside from the multiple proton transfer steps occurring during catalysis, decarboxylation of the tetrahedral substrate−ThDP adduct is a crucial reaction of the catalytic sequence. Independent of the substrate specific substituent (methyl, benzyl, or indolyl fragment) linked to the carbonyl fragment, decarboxylation is exclusively slowed in IPDC variants with substitutions in the Glu-Asp-His pattern, a structural motif that enfolds the thiazolium nucleus in the X-ray structure. The kinetic behavior of these variants leads us to conclude that the substrate-derived carboxylate is accommodated in this pocket. The resultant conformation shows a geometry in which the carboxylate fragment is above the plane of the conjugated thiazolium system (Figure 6). The positively charged thiazolium ring would then provide an optimal electron sink for stabilizing the pair of electrons released upon decarboxylation, being in accordance with the maximum-overlap mechanism proposed for pyridoxal phosphate- and ThDP-dependent enzymes. We learn that catalysis provided by the carboxylate pocket accounts for a 10^2-10^4-fold rate acceleration of decarboxylation. As the rate of the enzymic decarboxylation exceeds that of the nonenzymic reaction by approximately 7 orders of magnitude (*11*), the remaining 10^3-10^5fold acceleration must result from other factors, presumably from a low polarity of the active site. Kinetic ^{13}C isotope effect studies on PDC variants by Huskey and co-workers could provide evidence of a participation of the homologous Asp side chain in the decarboxylation step (*52*). A structural comparison of ThDP-dependent decarboxylases reveals that PDC from bacteria and from yeast and IPDC share this motif, whereas BFDC does not contain the acidic side chains but rather, in an orientation nearly identical to that of the thiazolium nucleus, a serine residue (compare panels A and B of Figure 1). Both structural investigations with the enzyme-bound inhibitor (*R*)-mandelate as well as kinetic studies with serine variants show that (i) the carboxylate fragment interacts with this serine and (ii) the serine is involved in the decarboxylation step in BFDC (*9*). In other ThDP enzymes that act on pyruvate like PFOR, AHAS, and POX, no equivalent pattern is found (*36*, *37*, *41*). This structural heterogeneity does not allow formulation of a general principle of decarboxylation in ThDP enzymes; however, some basic concepts have to be considered. To achieve the 10^7-fold rate acceleration, enzymes must either stabilize the transition state or destabilize the ground state. Apparently, the negative charge of the carbanion intermediate formed upon decarboxylation can be stabilized by the distal positive charge of the thiazolium ring most effectively, when the conformation of the intermediate allows conjugation of the π electrons of the cofactor and the orbital of the electron pair at C_α. To date, no X-ray structures of tetrahedral

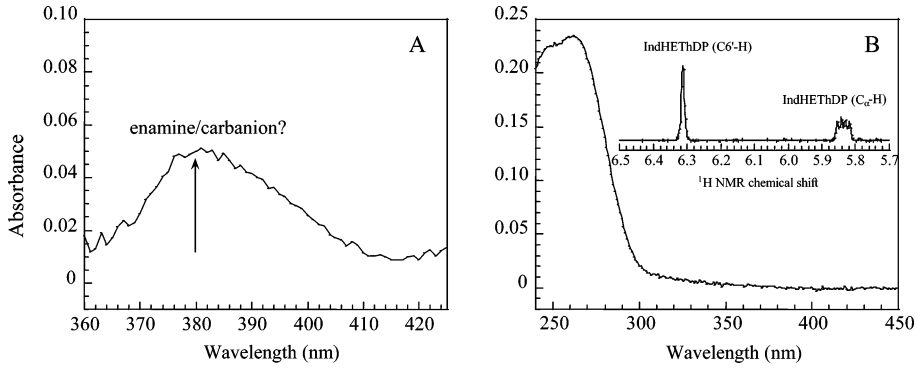

FIGURE 10: Detection of the elusive carbanion/enamine form of IndHEThDP during nonoxidative decarboxylation of Ipyr by IPDC variant Asp29Glu. (A) Section of the UV−vis absorbance spectrum of IPDC Asp29Glu (1 mg/mL) reacting with 1 mM Ipyr in 0.2 M MES at pH 6.5 and 30 °C after a reaction time of 2 min. The spectrum was corrected for individual contributions of the buffer, the substrate Ipyr, and the unreacted enzyme. The appearance of the new arising absorbance band at $\lambda_{max} \approx 380$ nm was assigned to the carbanion/enamine form of enzyme-bound IndHEThDP (see the text). (B) UV−vis absorption spectrum of the intermediates isolated from IPDC Asp29Glu reacting with Ipyr by acid quench (see Materials and Methods) and immediate pH readjustment from 0.75 to 6.5. The inset is a section of the ^{1}H NMR spectrum of isolated intermediates in Asp29Glu catalysis proving the exclusive accumulation of IndHEThDP.

substrate−ThDP adducts in an active site have been published, but in view of the NMR intermediate and carbon isotope effect studies, it is very likely that a perpendicular orientation of the carboxylate fragment is realized in the enzymes. According to model studies, this conformational control will give rise to a rate increase of 1 or 2 orders of magnitude (*53*) and could thus not solely explain the catalytic efficiency of ThDP enzymes. Since the nonenzymic decarboxylation of LThDP and analogous thiazolium compounds was shown to be faster in apolar solvents, it has been proposed that a less polar transition state (with respect to the ground state) will be effectively stabilized in a nonpolar environment, i.e., the active site. This factor may principally operate for POX and AHAS, but in ThDP decarboxylases with conceivable interactions of the substrate carboxylate with polar side chains (Glu-Asp-His motif in PDC and IPDC, Ser in BFDC), other factors may also be important. Although a truly compelling conclusion should await further structural and computational studies, the discussion at this point of some possibilities would seem to be justified. Considering the acidic side chains were ionized (Glu or/and Asp), the negative charge(s) would provide unfavorable interactions with the substrate carboxylate. Structural and computational studies on PLP enzymes and oritidine 5′-monophosphate decarboxylase (OMDase) confirmed that electrostatic stress may be an important factor in enzymic decarboxylation aside from stereochemical control (*54*−*57*). According to Jencks' famous Circe effect concept, favorable interactions of the substrate with the enzyme and cofactor shall lure the substrate into the active site and fix the leaving carboxylate in the vicinity of negatively charged side chains. The resultant charge repulsion was shown to account for the observed rates of decarboxylation in the different enzymes. If this situation applies for IPDC and PDC, a less polar transition state resembling the uncharged enamine/CO_2 couple would be stabilized promoting decarboxylation. But how could a simple ketoacid like pyruvate be lured into such an unfavorable environment? We speculate that the binding energy of the cofactor pays for the enforced *V* conformation and the concomitant activation of the aminopyrimidine shuttle, generating a high-energy carbanion species at C2, which ligates exergonically to the carbonyl fragment of the substrate. In effect, the binding energy of the cofactor may be used as a supportive driving force for a thermodynamically favorable reaction (C−C ligation) that in turn may lead to electrostatic stress of some part of the molecule being released upon decarboxylation. The catalytic trick of ThDP enzymes would be to enlarge a small substrate molecule with small binding energy by ligation to a larger and chemically reactive cofactor species, thus channeling the binding energy of the cofactor into chemical reactivity. The energy released in forming the tetrahedral substrate−ThDP adduct intermediate presumably will be also used for desolvation of the substrate. At least in part, some favorable interactions of the carboxylate fragment with the protein (histidine side chain) may help to decrease this energetic barrier. As Warshel emphasized, a preorganized dipolar environment in active sites of enzymes reducing the reorganization energy of relevant transition states is an important factor that contributes to the catalytic power of enzymes (*58*).

Reactivity and Chemical Fate of the Elusive Carbanion/Enamine. Finally, our results invite some speculation about how ThDP enzymes may control the chemical fate of the central carbanion/enamine intermediate. In ThDP decarboxylases, this key intermediate undergoes rapid protonation, a reaction that must be avoided by all other ThDP enzymes to allow either oxidation by electron acceptors or ligation with ketoacids, aldehydes, and sugars. Our studies on IPDC and PDC (*10*) suggest the Asp-His dyad or Glu-Asp-His triad of the carboxylate pocket to be vital for the protonation step of the carbanion/enamine in IPDC/PDC catalysis. A mutation of any of these residues slows the product release step by several orders of magnitude. In the X-ray structure of IPDC, these side chains constitute a highly organized hydrogen bond network; therefore, in view of the observed effects in the variants, an ultimate functional assignment should await further experiments. However, the observation of the IndHEThDP enamine in Asp29Glu tempted us to suggest a mechanism that mainly involves the Asp29-His115 pair. Alternatively, Glu468 may relay a proton from Asp29/His115 to the carbanion. As we have stated earlier in the Results, a carbanionic character of the conjugate base of the product−ThDP adduct will facilitate protonation whereas an enamine-like form will be more stable and disfavor protonation. Apparently, this pinpoints the dilemma with which ThDP decarboxylases have to deal. On one hand, a more neutral

transition state of decarboxylation is thought to account for much of the rate acceleration in enzymic catalysis, and on the other hand, the resultant enamine-like intermediate would require some destabilization to facilitate protonation. Probably, interactions of side chains with the intermediate may help to keep the α-OH and R substituent out of the thiazolium plane and prevent relaxation of the carbanion to the enamine. Considering the transition state of decarboxylation still possesses dipolar character (negatively charged carbanion and positively charged thiazolium), proton transfer may occur more easily (maybe late in the same transition state of decarboxylation as proposed for OMDase), but which factors would then account for the rate acceleration of enzymic decarboxylation? According to Warshel's concept, preoriented dipoles of the enzymic active site can effectively stabilize dipolar transition states and the gain in reorganization energy stored in the tertiary fold of the enzyme may be a tremendous catalytic factor, but obviously, the reactant state is also dipolar in ThDP-catalyzed decarboxylation, although with a different spatial orientation.

Finally, we have shown in this work that key intermediates invoked in enzymic decarboxylation of the ketoacids Pyr, BF, and Ipyr can be isolated, confirming the generality of Breslow's mechanism. The kinetic NMR analysis of wild-type IPDC and variants is useful in mapping interactions and catalytic contributions of side chains in the active site. On the basis of our data, we conclude that stereochemical control of decarboxylation is, besides a low-polar environment, an important factor in ThDP decarboxylases and that a highly evolved cofactor proton shuttle is involved in multiple proton transfer steps.

ACKNOWLEDGMENT

We gratefully acknowledge many stimulating discussions with Prof. Ron Kluger and Prof. Richard L. Schowen on mechanistic aspects of ThDP catalysis, their generous support, and their incessant interest in our work.

REFERENCES

1. Koga, J., Adachi, T., and Hidaka, H. (1992) Purification and characterization of indolepyruvate decarboxylase. A novel enzyme for indole-3-acetic acid biosynthesis in *Enterobacter cloacae*, *J. Biol. Chem. 267*, 15823−15828.
2. Kawaguchi, M., and Syono, K. (1996) The excessive production of indole-3-acetic acid and its significance in studies of the biosynthesis of this regulator of plant growth and development, *Plant Cell Physiol. 37*, 1043−1048.
3. Patten, C. L., and Glick, B. R. (1996) Bacterial biosynthesis of indole-3-acetic acid, *Can. J. Microbiol. 42*, 207−220.
4. Schütz, A., Golbik, R., Tittmann, K., Svergun, D. I., Koch, M. H., Hübner, G., and König S. (2003) Studies on structure−function relationships of indolepyruvate decarboxylase from *Enterobacter cloacae*, a key enzyme of the indole acetic acid pathway, *Eur. J. Biochem. 270*, 2322−2331.
5. Schütz, A., Sandalova, T., Ricagno, S., Hübner, G., König, S., and Schneider, G. (2003) Crystal structure of thiamindiphosphate-dependent indolepyruvate decarboxylase from *Enterobacter cloacae*, an enzyme involved in the biosynthesis of the plant hormone indole-3-acetic acid, *Eur. J. Biochem. 270*, 2312−2321.
6. Dobritzsch, D., König, S., Schneider, G., and Lu, G. (1998) High-resolution crystal structure of pyruvate decarboxylase from *Zymomonas mobilis*. Implications for substrate activation in pyruvate decarboxylases, *J. Biol. Chem. 273*, 20196−20204.
7. Hasson, M. S., Muscate, A., McLeish, M. J., Polovnikova, L. S., Gerlt, J. A., Kenyon, G. L., Petsko, G. A., and Ringe, D. (1998) The crystal structure of benzoylformate decarboxylase at 1.6 Å resolution: Diversity of catalytic residues in thiamin diphosphate-dependent enzymes, *Biochemistry 37*, 9918−9930.
8. Sergienko, E. A., Wang, J., Polovnikova, L., Hasson, M. S., McLeish, M. J., Kenyon, G. L., and Jordan, F. (2000) Spectroscopic detection of transient thiamin diphosphate-bound intermediates on benzoylformate decarboxylase, *Biochemistry 39*, 13862−13869.
9. Polovnikova, E. S., McLeish, M. J., Sergienko, E. A., Burgner, J. T., Anderson, N. L., Bera, A. K., Jordan, F., Kenyon, G. L., and Hasson, M. S. (2003) Structural and kinetic analysis of catalysis by a thiamin diphosphate-dependent enzyme, benzoylformate decarboxylase, *Biochemistry 42*, 1820−1830.
10. Tittmann, K., Golbik, R., Uhlemann, K., Khailova, L., Schneider, G., Patel, M., Jordan, F., Chipman, D. M., Duggleby, R. G., and Hübner, G. (2003) NMR analysis of covalent intermediates in thiamin diphosphate enzymes, *Biochemistry 42*, 7885−7891.
11. Kluger, R., Chin, J., and Smyth, T. (1981) Thiamin-catalyzed decarboxylation of pyruvate. Synthesis and reactivity of the central, elusive intermediate, α-lactylthiamin, *J. Am. Chem. Soc. 103*, 884−888.
12. Kluger, R. (1987) Thiamin diphosphate: A mechanistic update on enzymic and nonenzymic catalysis of decarboxylation, *Chem. Rev. 87*, 863−876.
13. Turano, A., Furey, W., Pletcher, J., Sax, M., Pike, D., and Kluger, R. (1982) Synthesis and structure of an analogue of 2-(α-lactyl)-thiamin, racemic methyl 2-hydroxy-2-(2-thiamin)ethylphosphonate chloride trihydrate. A conformation for a least-motion, maximum-overlap mechanism for thiamin catalysis, *J. Am. Chem. Soc. 104*, 3089−3095.
14. Friedemann, R., and Breitkopf, C. (1996) Theoretical studies on the decarboxylation reaction in thiamin catalysis, *Int. J. Quantum Chem. 57*, 943−948.
15. Lobell, M., and Crout, D. H. G. (1996) Pyruvate Decarboxylase: A molecular modeling study of pyruvate decarboxylation and acyloin formation, *J. Am. Chem. Soc. 118*, 1867−1873.
16. Tung, W. L., and Chow, K. C. (1995) A modified medium for efficient electrotransformation of *E. coli*, *Trends Genet. 11*, 128−129.
17. Bradford, M. M. (1976) A rapid and sensitive method for the quantitation of microgram quantities of protein utilizing the principle of protein-dye binding, *Anal. Biochem. 72*, 248−254.
18. Hallmann, G., and Hägle, H. (1963) Benzofuranderivate: Tryptamin-, Serotonin- und Melatonin-Analoga, *Liebigs Ann. Chem. 662*, 147−159.
19. Krampitz, L. O., Greull, G., Miller, C. S., Bicking, J. B., Skeggs, H. R., and Sprague, J. M. (1958) An active acetaldehyde-thiamine intermediate, *J. Am. Chem. Soc. 80*, 5893−5894.
20. Mieyal, J. J., Bantle, G., Votaw, R. G., Rosner, I. A., and Sable, H. Z. (1971) Coenzyme interactions. V. The second carbanion in reactions catalyzed by thiamine, *J. Biol. Chem. 246*, 5213−5219.
21. Jordan, F., Li, H., and Brown, A. (1999) Remarkable stabilization of zwitterionic intermediates may account for a billion-fold rate acceleration by thiamin diphosphate-dependent decarboxylases, *Biochemistry 38*, 6369−6373.
22. Alvarez, F., Ermer, J., Hübner, G., Schellenberger, A., and Schowen, R. L. (1991) Catalytic power of pyruvate decarboxylase. Rate-limiting events and microscopic rate constants from primary carbon and secondary hydrogen isotope effects, *J. Am. Chem. Soc. 113*, 8403−8409.
23. Sun, S., Duggleby, R. G., and Schowen, R. L. (1995) Linkage of catalysis and regulation in enzyme action. Carbon isotope effects, solvent isotope effects, and proton inventories for the unregulated pyruvate decarboxylase of *Zymomonas mobilis*, *J. Am. Chem. Soc. 117*, 7317−7322.
24. Weiss, P. M., Garcia, G. A., Kenyon, G. L., and Cleland, W. W. (1988) Kinetics and mechanism of benzoylformate decarboxylase using ^{13}C and solvent deuterium isotope effects on benzoylformate and benzoylformate analogues, *Biochemistry 27*, 2197−2205.
25. Kern, D., Kern, G., Neef, H., Tittmann, K., Killenberg-Jabs, M., Wikner, C., Schneider, G., and Hübner, G. (1997) How thiamine diphosphate is activated in enzymes, *Science 275*, 67−70.
26. Hübner, G., Tittmann, K., Killenberg-Jabs, M., Schäffner, J., Spinka, M., Neef, H., Kern, D., Kern, G., Schneider, G., Wikner, C., and Ghisla, S. (1998) Activation of thiamin diphosphate in enzymes, *Biochim. Biophys. Acta 1385*, 221−228.
27. Jordan, F., Nemeria, N. S., Zhang, S., Yan, Y., Arjunan, P., and Furey, W. (2003) Dual catalytic apparatus of the thiamin diphosphate coenzyme: Acid−base via the 1′,4′-iminopyrimidine tau-

tomer along with its electrophilic role, *J. Am. Chem. Soc. 125*, 12732−12738.
28. Nemeria, N., Baykal, A., Joseph, E., Zhang, S., Yan, Y., Furey, W., and Jordan, F. (2004) Tetrahedral intermediates in thiamin diphosphate-dependent decarboxylations exist as a 1′,4′-imino tautomeric form of the coenzyme, unlike the Michaelis complex or the free coenzyme, *Biochemistry 43*, 6565−6575.
29. Tittmann, K., Vyazmensky, M., Hübner, G., Barak, Z., and Chipman, D. M. (2005) The carboligation reaction of acetohydroxyacid synthase II. Steady-state intermediate distribution in wild-type and mutants by NMR, *Proc. Natl. Acad. Sci. U.S.A. 102*, 553−558.
30. Kluger, R., Hu, Q., and Moore, I. F. (2004) Benzoylformatedecarboxylase: Intermediates, transition states, and diversions, in *Thiamine. Catalytic Mechanisms in Normal and Disease States* (Jordan, F., and Patel, M. S., Eds.) pp 291−308, Marcel Dekker, New York.
31. Hu, Q., and Kluger, R. (2002) Reactivity of intermediates in benzoylformate decarboxylase: Avoiding the path to destruction, *J. Am. Chem. Soc. 124*, 14858−14859.
32. Crosby, J., and Lienhard, G. E. (1970) Mechanisms of thiamine-catalyzed reactions. A kinetic analysis of the decarboxylation of pyruvate by 3,4-dimethylthiazolium ion in water and ethanol, *J. Am. Chem. Soc. 92*, 5707−5716.
33. Schowen, R. L. (1998) Thiamin-dependent enzymes, in *Comprehensive Biological Catalysis* (Sinnot, M., Ed.) Vol. 2, pp 217−266, Academic Press, London.
34. Hu, Q., and Kluger, R. (2004) Fragmentation of the conjugate base of 2-(1-hydroxybenzyl)thiamin: Does benzoylformate decarboxylase prevent orbital overlap to avoid it? *J. Am. Chem. Soc. 126*, 68−69.
35. Lindqvist, Y., Schneider, G., Ermler, U., and Sundström, M. (1992) Three-dimensional structure of transketolase, a thiamine diphosphate dependent enzyme, at 2.5 Å resolution, *EMBO J. 11*, 2373−2379.
36. Muller, Y. A., and Schulz, G. E. (1993) Structure of the thiamine- and flavin-dependent enzyme pyruvate oxidase, *Science 259*, 965−967.
37. Pang, S. S., Duggleby, R. G., and Guddat, L. W. (2002) Crystal structure of the catalytic subunit of yeast acetohydroxyacid synthase: A target for herbidical inhibitors, *J. Mol. Biol. 317*, 249−262.
38. Arjunan, P., Umland, T., Dyda, F., Swaminathan, S., Furey, W., Sax, M., Farrenkopf, B., Gao, Y., Zhang, D., and Jordan, F. (1996) Crystal structure of the thiamine diphosphate-dependent enzyme pyruvate decarboxylase from the yeast *Saccharomyces cerevisiae* at 2.3 Å resolution, *J. Mol. Biol. 256*, 590−600.
39. Arjunan, P., Nemeria, N., Brunskill, A., Chandrasekhar, K., Sax, M., Yan, Y., Jordan, F., Guest, J. R., and Furey, W. (2002) Structure of the pyruvate dehydrogenase multienzyme complex E1 component from *Escherichia coli* at 1.85 Å resolution, *Biochemistry 41*, 5213−5221.
40. Ciszak, E. M., Korotchkina, L. G., Dominiak, P. M., Sidhu, S., and Patel, M. S. (2003) Structural basis for flip-flop action of thiamin pyrophosphate-dependent enzymes revealed by human pyruvate dehydrogenase, *J. Biol. Chem. 278*, 21240−21246.
41. Chabriere, E., Charon, M. H., Volbeda, A., Pieulle, L., Hatchikian, E. C., and Fontecilla-Camps, J. C. (1999) Crystal structures of the key anaerobic enzyme pyruvate:ferredoxin oxidoreductase, free and in complex with pyruvate, *Nat. Struct. Biol. 6*, 182−190.
42. Chabriere, E., Vernede, X., Guigliarelli, B., Charon, M. H., Hatchikian, E. C., and Fontecilla-Camps, J. C. (2001) Crystal structure of the free radical intermediate of pyruvate:ferredoxin oxidoreductase, *Science 294*, 2559−2563.
43. Fiedler, E., Thorell, S., Sandalova, T., Golbik, R., König, S., and Schneider, G. (2002) Snapshot of a key intermediate in enzymatic thiamin catalysis: Crystal structure of the α-carbanion of (α,β-dihydroxyethyl)-thiamin diphosphate in the active site of transketolase from *Saccharomyces cerevisiae*, *Proc. Natl. Acad. Sci. U.S.A. 99*, 591−595.
44. Tittmann, K., Golbik, R., Ghisla, S., and Hübner, G. (2000) Mechanism of elementary catalytic steps of pyruvate oxidase from *Lactobacillus plantarum*, *Biochemistry 39*, 10747−10754.
45. Menon, S., and Ragsdale, S. W. (1997) Mechanism of the *Clostridium thermoaceticum* pyruvate:ferredoxin oxidoreductase: Evidence for the common catalytic intermediacy of the hydroxyethylthiamine pyropyrosphate radical, *Biochemistry 36*, 8484−8494.
46. Sergienko, E. A., and Jordan, F. (2001) Catalytic acid−base groups in yeast pyruvate decarboxylase. 2. Insights into the specific roles of D28 and E477 from the rates and stereospecificity of formation of carboligase side products, *Biochemistry 40*, 7369−7381.
47. Bar-Ilan, A., Balan, V., Tittmann, K., Golbik, R., Vyazmensky, M., Hübner, G., Barak, Z., and Chipman, D. M. (2001) Binding and activation of thiamin diphosphate in acetohydroxyacid synthase, *Biochemistry 40*, 11946−11954.
48. Liu, M., Sergienko, E. A., Guo, F., Wang, J., Tittmann, K., Hübner, G., Furey, W., and Jordan, F. (2001) Catalytic acid−base groups in yeast pyruvate decarboxylase. 1. Site-directed mutagenesis and steady-state kinetic studies on the enzyme with the D28A, H114F, H115F, and E477Q substitutions, *Biochemistry 40*, 7355−7368.
49. Nakai, T., Nakagawa, N., Maoka, N., Masui, R., Kuramitsu, S., and Kamiya, N. (2004) Ligand-induced conformational changes and a reaction intermediate in branched-chain 2-oxo acid dehydrogenase (E1) from *Thermus thermophilus* HB8, as revealed by X-ray crystallography, *J. Mol. Biol. 337*, 1011−1033.
50. Wille, G., Meyer, D., Bange, G., Steinmetz, A., König, S., Hübner, G., and Tittmann, K. (2005) (manuscript in preparation).
51. Washabaugh, M. W., and Jencks, W. P. (1988) Thiazolium C2-proton exchange. Structure−reactivity correlations and the pK_a of thiamin C2-H revisited, *Biochemistry 27*, 5044−5053.
52. Chen, L., Yuan, Y., and Huskey, P. W. (2004) Transition-state responses to amino acid perturbations in yeast pyruvate decarboxylase: A carbon kinetic isotope effect study, *J. Phys. Org. Chem. 17*, 572−578.
53. Jencks, W. P. (1975) Binding energy, specificity, and enzymic catalysis: The circe effect, *Adv. Enzymol. Relat. Areas Mol. Biol. 43*, 219−410.
54. Wu, N., Mo, Y., Gao, J., and Pai, E. F. (1998) Electrostatic stress in catalysis: Structure and mechanism of the enzyme orotidine monophosphate decarboxylase, *Proc. Natl. Acad. Sci. U.S.A. 97*, 2017−2022.
55. Dunathan, H. C. (1971) Stereochemical aspects of pyridoxal phosphate catalysis, *Adv. Enzymol. Relat. Areas Mol. Biol. 35*, 79−134.
56. Jackson, L. K., Brooks, H. B., Myers, D. P., and Phillips, M. A. (2003) Ornithine decarboxylase promotes catalysis by binding the carboxylate in a buried pocket containing phenylalanine 397, *Biochemistry 42*, 2933−2940.
57. Cheong, C. G., Escalante-Semerena, J. C., and Rayment, I. (2002) Structural studies of the L-threonine-*O*-3-phosphate decarboxylase (CobD) enzyme from *Salmonella enterica*: The apo, substrate, and product-aldimine complexes, *Biochemistry 41*, 9079−9089.
58. Warshel, A., and Florian, J. (1998) Computer simulations of enzyme catalysis: Finding out what has been optimized by evolution, *Proc. Natl. Acad. Sci. U.S.A. 95*, 5950−5955.
59. Humphrey, W., Dalke, A., and Schulten, K. (1996) VMD: Visual molecular dynamics, *J. Mol. Graphics 14*, 33−38.

BI0473354